Journal of Materials Chemistry A

REVIEW

View Article Online
View Journal | View Issue

Cite this: J. Mater. Chem. A, 2015, 3, 16896

The rise of hematite: origin and strategies to reduce the high onset potential for the oxygen evolution reaction

Beniamino Iandolo,†* Björn Wickman, Igor Zorić and Anders Hellman*

Received 7th May 2015
Accepted 12th June 2015

DOI: 10.1039/c5ta03362d

www.rsc.org/MaterialsA

Hematite (α-Fe_2O_3) has emerged as a promising material for photoelectrochemical (PEC) water splitting thanks to its abundance, stability in an aqueous environment, favorable optical bandgap and position of the electronic valence band. Nevertheless, its performance as a photoanode is considerably lower than what is theoretically achievable. In particular, the high electrochemical potential usually needed to initiate water oxidation is detrimental to the prospect of using hematite for practical devices. In this review we elucidate the appealing, as well as the challenging, aspects of using hematite for PEC water splitting and focus on the recent efforts towards lowering the onset potential of water oxidation. We examine and rationalize several strategies pursued to achieve this goal involving manipulation of the hematite/electrolyte interface, as well as improving relevant properties of hematite itself.

Introduction

Fossil fuels account for about 87% of the global mean power consumption, which is currently about 16 terawatt (TW)[1,2] and is expected to increase up to 30 TW by 2050.[3,4] It follows that any technology for harvesting, converting and/or storing energy in a sustainable way must be scaled to the TW level in order to make an appreciable impact at a global scale. Solar energy is the most appealing candidate to solve this appropriately called "TW challenge".[5] More energy, in the form of sunlight, strikes the Earth in one hour than what society currently consumes in a year.[6] However, sunlight is intermittent, *i.e.*, it varies irregularly over the day, year, and place on earth, which implies that schemes and devices to store and release the harvested energy on demand are needed. An elegant approach to this problem consists in directly converting sunlight into chemical energy in the form of molecular bonds, *i.e.* producing fuels. Nature has already implemented such a scheme in biological photosynthesis, where sunlight converts CO_2 and H_2O into hydrocarbons and O_2. However, since the overall efficiency of this process is low (about 1% at best),[7,8] different routes towards artificial photosynthesis have received considerable attention.[9] In

Department of Applied Physics, Chalmers University of Technology, SE-41296 Göteborg, Sweden. E-mail: anders.hellman@chalmers.se

† Current address: Center for Electron Nanoscopy, Technical University of Denmark, DK-2800 Kgs. Lyngby, Denmark.

Dr Beniamino Iandolo obtained his Ph.D. in Physics from the Chalmers University of Technology, Sweden, in 2014. Research for his doctoral thesis centered on light-driven water splitting on hematite. He is currently a postdoctoral fellow at the Technical University of Denmark, where he scrutinizes novel materials for solar energy conversion and storage using environmental transmission electron microscopy.

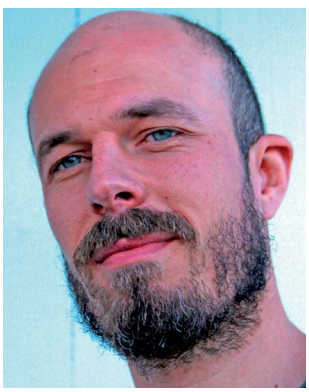

Dr Björn Wickman is a postdoctoral fellow at Chalmers University of Technology, Sweden. He received his Ph.D. in Physics from Chalmers University of Technology in 2010. Dr Wickman has done postdoctoral studies at the Technical University of Denmark. His research interests center around electro- and photoelectrochemical solutions for energy and environmental applications. He has developed and evaluated well controlled, nanofabricated model systems to study reaction mechanisms in the fields of fuel cells, CO_2 reduction, and water splitting.

particular, H_2 production from H_2O splitting has the potential to become the backbone of a hydrogen-based sustainable energy economy,[10,11] given the abundance of H_2O on Earth and that the only byproduct of H_2 when consumed in a fuel cell is, once again, H_2O.

One can identify three types of devices to perform solar water splitting: (i) photovoltaic (PV) devices wired to H_2O electrolyzers, (ii) photocatalytic cells, and (iii) photoelectrochemical (PEC) cells. The latter ones use solid-state electrodes in a similar way to conventional electrolyzers, where H_2O oxidation (or O_2 evolution reaction, OER) and reduction (H_2 evolution reaction, HER) take place at two different solid/liquid junctions. In PEC cells, at least one of the electrodes consists of a semiconductor capable of absorbing the incoming light, and in which a depletion (or space-charge, SC) region is formed at equilibrium. The photogenerated charges are separated by the electric field in the SC region and travel to a solid/liquid junction where they take part in either the HER or the OER.

The key requirements of materials for high-efficiency PEC water splitting can be summarized as follows:

- Bandgap size that allows for broad light absorption.
- Quasi-Fermi energy levels for electrons and holes that straddle the HER and OER potential respectively.
- High yield of conversion of photogenerated charges into H_2 and O_2.

Moreover, the electrodes must be durable in the often harsh electrolytic environment and consist of earth abundant elements in view of process scalability. Despite the enormous effort since the seminal work on water splitting on TiO_2,[12,13] no single material that meets all these requirements has emerged so far.[14,15] While much work is devoted to identify the ideal semiconductor for this purpose (also using combinatorial and/or *ab initio* calculations[16–18]), focus is increasingly shifting towards using two or more photoactive materials. A commonly investigated scheme involves coupling a semiconductor capable of carrying out one of the half-reactions to a PV device that supplies the bias needed to perform complete water splitting.[14] III–V photocathodes in connection to a PV cell reach solar-to-hydrogen (STH) conversion efficiency over 12%,[19] although cost and stability considerations have prevented these devices from attaining economic significance. Alternatively, a stable, inexpensive metal oxide can be used to perform the OER. Metal oxides commonly used within this scheme are TiO_2,[20–24] WO_3,[25–29] ZnO,[30–33] $BiVO_4$ [34–38] and Fe_2O_3.[39–43]

Fe_2O_3 (or iron(III) oxide, hematite) is of great interest thanks to its bandgap of ~2.0 eV, which results in a theoretical maximum STH conversion efficiency of about 15%.[44] However, the highest STH efficiency achieved so far is 3.1% using state-of-the-art hematite photoanodes,[45] whereas more typically STH is of the order of about 1% or less.[11] Clearly, much remains to be done in order to exploit the full potential of hematite. In this review, we briefly describe the properties of hematite of interest for PEC water splitting. Then, we focus on one of the factors limiting the performance of hematite, namely the highly anodic potential required to initiate the OER. We critically examine the advancements in alleviating the former issue, as well as review recent efforts in deepening the understanding of the OER on hematite.

Hematite for PEC water splitting

In the search for the ultimate semiconductor for PEC water splitting, hematite attracted interest almost four decades ago.[46] This fact is not surprising given (i) that hematite can theoretically absorb up to 40% of solar radiation,[47] (ii) that it shows excellent (photo)electrochemical stability in a pH range from 3 to 14,[48] and (iii) that iron is the fourth most abundant element in the Earth's crust.[2] Hematite is thermodynamically the most stable form of iron oxide, and all iron oxides can be transformed into hematite upon appropriate thermal treatment.[49,50] In the following section, we briefly review the PEC properties of

Igor Zorić is a Professor Emeritus at the Department of Applied Physics, Chalmers University of Technology, Sweden. His work focuses on dynamics and kinetics of surface reactions, nanoplasmonics and photoelectrochemistry.

Anders Hellman is an Associate Professor at the Department of Applied Physics, Chalmers University of Technology, Sweden. He received his Ph.D. in Physics in 2003 from the University of Gothenburg, Sweden. Dr Hellman has done postdoctoral studies at Haldor Topsøe A/S, Technical University of Denmark, and at the Competence Centre for Catalysis, Sweden. He has worked on various topics related to surface science, heterogeneous catalysis and materials for energy harvesting, such as charge transfer and non-adiabaticity in surface reactions, ammonia synthesis, CO and methane oxidation, thin oxides supported on metals, and (photo) electrochemical studies of water splitting.

hematite. Then, we outline the challenges in exploiting the full potential of hematite as a photoanode.

PEC properties

The optical and electronic properties of hematite have been thoroughly investigated and are summarized in recent reviews.[51–53] The optical bandgap energy is reported between 1.9 and 2.2 eV (corresponding to wavelengths of 650 and 560 nm respectively) depending on the sample preparation technique.[51] Tauc's analysis[54] of the absorption coefficient indicates that the bandgap is indirect, *i.e.* phonon participation is necessary in the photoexcitation process. As a consequence, the absorption length α^{-1} in hematite is relatively long, for instance, $\alpha^{-1} =$ 118 nm at a photon wavelength of 550 nm.[55]

In terms of electronic properties, hematite is described as a Mott insulator[56] where charge transport takes place *via* polaron hopping,[57,58] using models that include the effect of the size difference between Fe^{2+} and Fe^{3+} ions and the associated lattice distortion.[59,60] Notably, the electron conduction within the (0001) basal plane is four orders of magnitude higher than in the perpendicular planes.[61–63] Femtosecond laser spectroscopy studies of the excited states in hematite nanoparticles, thin films and single crystals reveal an ultra-fast dynamics, where hot electrons thermalize within 300 fs and recombine within 3 ps.[64,65] Based on the short lifetime and low charge carrier mobility value,[66] the diffusion length for holes L_D is usually estimated to be between 1.5 and 5 nm.[67,68]

The OER involves four holes for each O_2 molecule produced, with a characteristic time for a complete cycle as long as some seconds on hematite,[69] and hence it is usually characterized as "slow" or "sluggish". The microscopic mechanism of the OER on hematite is currently the subject of intense investigation.[70–73] A few schemes involving different reaction intermediates have been proposed,[39,69,74] and the recent review by Young *et al.*[52] summarizes the advancement on the topic. The formation of some reaction intermediates such as Fe–O and Fe–OOH is consistent with the hypothesis that the OER proceeds *via* the trapping of holes at Fe species, and subsequent transfer of these holes to the electrolyte.[74,75] These states are often referred to as surface states, and have been probed using several spectroscopic techniques such as electrochemical impedance spectroscopy (EIS),[74,75] intensity modulated photocurrent spectroscopy (IMPS),[76,77] light/potential modulated absorbance spectroscopy (LMAS/PMAS)[78,79] and transient absorption spectroscopy (TAS).[69,80] The surface states were initially regarded to act solely as recombination centers, with the OER proceeding *via* direct transfer of holes from the valence band. On the other hand, there is increasing evidence that the OER actually takes place from the same surface states, which therefore display an ambivalent nature. For instance, thanks to a combination of first-principle calculations and PEC measurements on polycrystalline hematite thin films, it was demonstrated that the surface states act as recombination centers for potentials more cathodic than the onset potential, V_{onset}, while as states through which the OER takes place for potentials more anodic than V_{onset}.[81]

Challenges

Fig. 1a shows a schematic energy diagram of a PEC water splitting device based on a hematite photoanode and a metallic cathode. Photons with energy equal to or larger than the bandgap energy E_G are absorbed with efficiency η_{e^-/h^+}. The quasi-Fermi energy levels for electrons and holes are indicated as $E_{F,n}$ and $E_{F,p}$, respectively. The difference between the two equals the photovoltage sustained by hematite, V_{ph}. The built-in electric field extends throughout the depletion region (characterized by a length W_{SC}) and drives holes towards the hematite/electrolyte junction and electrons to the cathode *via* an electron collector and an external circuit. The flat band potential V_{fb} of hematite (not shown here) is the potential at which there is no built-in field and therefore no band bending in the semiconductor. η_{tr} is the fraction of photogenerated charges

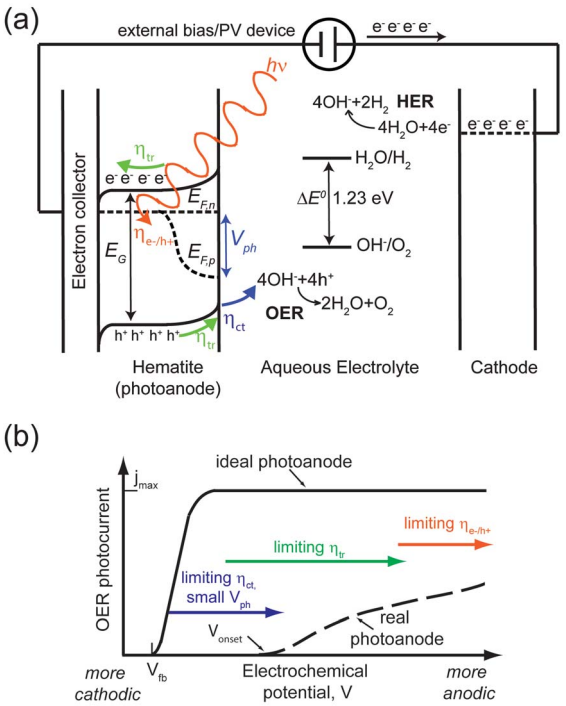

Fig. 1 (a) Schematic energy diagram of a PEC device based on a hematite photoanode. Photons with energy equal to or larger than the bandgap in hematite E_G are absorbed with efficiency η_{e^-/h^+}. The built-in electric field in hematite drives holes towards the hematite/electrolyte junction and electrons to the cathode (usually *via* a charge collector and an external circuit). η_{tr} is the fraction of photogenerated charges reaching the respective solid/liquid interface. Holes are transferred to the electrolyte with efficiency η_{ct}, and take part in the OER. An external bias/PV device supplies electrons with sufficient energy so that they take part in the HER. (b) PEC performance gap between a state-of-the-art photoanode and the ideal hematite-based photoanode. The former (dashed line) shows an OER V_{onset} between 1.0 and 1.1 V *vs.* RHE and slowly reaches a maximum photocurrent j_{max} of 4 mA cm^{-2} at 1.5 V *vs.* RHE. In the latter (solid line), $V_{onset} = V_{fb}$ (typically 0.5 V *vs.* RHE) and a j_{max} of 12 mA cm^{-2} is reached within 0.1 V. The arrows indicate the *main* performance limiting factor for increasingly anodic potential: first charge transfer at the hematite/electrolyte interface and the small photovoltage, then charge transport within hematite, finally photon absorption in the semiconductor.

reaching the respective solid/liquid interface. Then, holes are transferred to the electrolyte with efficiency η_{ct}, and take part in the OER. The overall STH efficiency of the device is determined by the following: (i) charge generation efficiency η_{e^-/h^+}; (ii) charge transport efficiency η_{tr}; (iii) charge transfer efficiency η_{ct}; (iv) oxidative power of holes; (v) reducing power of electrons.

Achieving high η_{e^-/h^+} and η_{tr} simultaneously is challenging given the mismatch between α^{-1} and $W_{SC} + L_D$.[82–84] While the electron conductivity can be increased by introducing dopant atoms (at levels of around a few percent) with higher valence than 3+ (ref. 85–98) or oxygen vacancies,[99] even in a heavy doping regime $\alpha^{-1} \gg W_{SC} + L_D$, since W_{SC} shortens for increasing dopant concentration.[100] Fabrication of nanostructured electrodes has shown to be effective in alleviating this mismatch, and a plethora of morphologies has been demonstrated in the last decade.[41,95,101–114] Another promising strategy consists in employing ultrathin (*i.e.* thickness smaller than 50 nm) hematite films and enhancing η_{e^-/h^+} through improving photon management by depositing hematite on top of a reflecting surface,[115] or by sensitizing it with nanostructures supporting plasmonic resonances.[116–123]

η_{ct} is normally close to unity only when a high anodic potential is applied to hematite, due to the slow OER kinetics mentioned above. Moreover, V_{ph} is usually much lower than the theoretical maximum. For heavily doped hematite, ideally, $E_{F,n}$ lies just below the bottom of the conduction band and V_{ph} almost equals the optical bandgap, leaving $E_{F,p}$ just above the top of the valence band. Unfortunately, this is far from being the case for hematite, where V_{ph} is typically smaller than 0.4 eV.[124] We emphasize that the small V_{ph} is largely overlooked when considering the performance-limiting factors of hematite, since it is often assumed that the latter is an excellent candidate for the OER based on the consideration that the *top of the valence band* lies about 0.7 eV below the OER potential.[53]

Finally, UV photoelectron spectroscopy indicates that the bottom of the conduction band lies 0.1–0.2 eV lower than the HER potential.[125] Therefore, even for heavily n-doped hematite where the quasi-Fermi for electrons in $E_{F,n}$ lies just below the bottom of the conduction band, complete water splitting using hematite as a single photoabsorber cannot take place without an external bias.[14,126–128]

Focusing on the OER half-cell reaction (and therefore neglecting here overpotentials and other issues associated with the HER), the non-idealities mentioned above result in a considerable discrepancy between the theoretical maximum performance of a hematite photoanode and the one normally observed. This discrepancy can be summarized in a plot of photocurrent *vs.* electrochemical potential (or $j(V)$ plot), as illustrated in Fig. 1b. Here, the plateau photocurrent j_{max} is the maximum photocurrent in the optical limit where all the photons with energy higher than E_G are absorbed and all the generated holes are consumed in the OER. Under these assumptions, j_{max} would equal 12 mA cm^{-2}.[93] In the ideal photoanode, the onset potential V_{onset} equals the flat band potential V_{fb}, and the photocurrent reaches j_{max} within 0.1 V from V_{onset}, whereas it typically takes 0.4–0.5 V to reach j_{max}.[51] As illustrated in Fig. 1b, it is possible to identify three regions where some of the aforementioned processes are the *main* performance limiting factors:

1. For $V_{fb} < V < V_{onset}$, η_{ct} and the small V_{ph} are the bottlenecks.

2. For V moderately more anodic than V_{onset}, η_{tr} limits the reaction.

3. For V highly more anodic than V_{onset}, the performance is only limited by η_{e^-/h^+}.

State-of-the-art nanostructured hematite photoanodes show a V_{onset} of around 1.1 V *vs.* the reversible hydrogen electrode (RHE), reaching a j_{max} of about 4 mA cm^{-2} at 1.5 V *vs.* RHE.[114] The potential at which j_{max} is reached is unacceptably high, given that V_{fb} is normally between 0.4 and 0.6 V *vs.* RHE. An extra price of around 1 V *for each hole* is simply too large, as it requires the addition of more PV devices to provide additional photovoltage. The lowering of V_{onset} is therefore a key issue to tackle in order to increase the chances of hematite based PEC water splitting to attain practical significance. In the remainder of this manuscript, we will present and critically review the strategies to lower the OER V_{onset} on hematite.

Lowering V_{onset} of the OER

From the discussion of the PEC properties of hematite carried out in the previous section, it is clear that the OER V_{onset} can be modified by altering several properties of the photoanode. The latter ones are schematically illustrated in Fig. 2a: bulk charge recombination (at the rate $k_{rec,bulk}$), charge recombination at the hematite/electrolyte interface (at the rate $k_{rec,surf}$), hole transfer from the semiconductor to electrolyte (at the rate k_{ct}), photovoltage V_{ph} and flat band potential V_{fb}. The OER is assumed here to take place *via* surface states. Nevertheless, the same rationale is applicable to photoanodes where the reaction proceeds *via* direct transfer of holes from the valence band. The different thickness of the arrows indicates the poor overall performance of hematite (especially for more cathodic potentials). Panels (b) to (f) in Fig. 2 illustrate *conceptually* how the situation can be improved by addressing these issues individually: (b) k_{ct} is increased, *i.e.* the OER kinetics is accelerated; (c) $k_{rec,surf}$ is suppressed; (d) $k_{rec,bulk}$ is reduced (this may also be achieved by reducing charge recombination at the interface between hematite and the electron collector, which is often a transparent conducting oxide); (e) V_{ph} is increased, thus enhancing the oxidative power of holes; (e) V_{fb} is lowered.

In order to improve one (or more) of the aforementioned properties and thus to lower V_{onset}, several approaches have been tested *experimentally*, as summarized in Table 1. It is clear that there are recurring strategies in the field, such as: doping hematite, introducing overlayers on top of hematite, or other (oxide) layers between hematite and the electron collector/substrate. As one can expect, and as we will discuss in what follows, modifying hematite by one technique in order to modify one particular property often affects other characteristics of the electrode, not necessarily in a beneficial way and sometimes leading to a decrease in overall performance.

Before we proceed to a more detailed description of the strategies outlined earlier, we mention that different methods

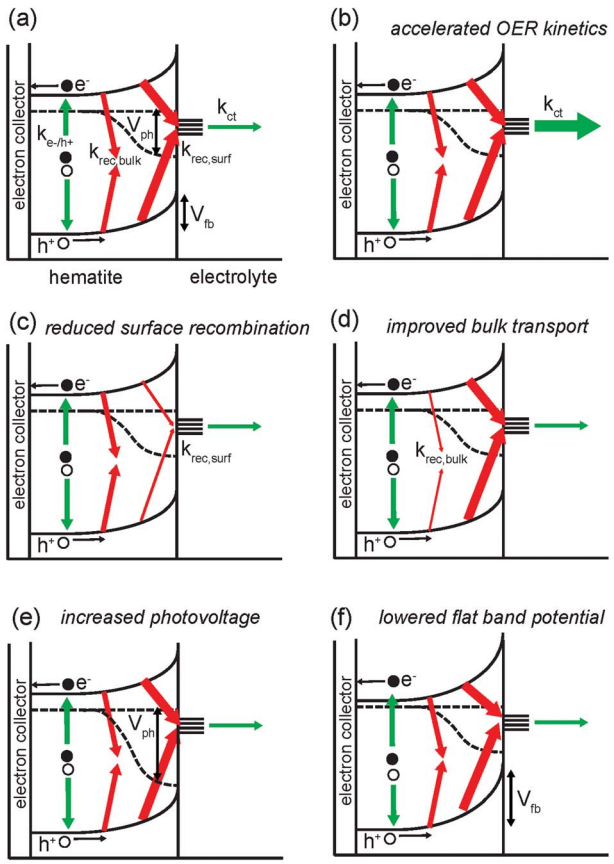

Fig. 2 (a) Schematics of PEC processes in the bulk of hematite and at the hematite/electrolyte interface for potentials more anodic than the flat band potential V_{fb}. Green arrows indicate desirable processes: photon absorption and consequent electron–hole pair generation (at a rate k_{e^-/h^+}) and charge transfer to the electrolyte (assumed to take place here from surface states) at a rate k_{ct}. Red arrows, instead, denote unwanted processes: charge recombination in the bulk (at a rate $k_{rec,bulk}$) and at the solid/liquid junction (at a rate $k_{rec,surf}$). The thickness of the arrows indicates the relative importance of the above mentioned processes in a typical hematite photoanode, resulting in highly anodic values of OER V_{onset}. Panels (b–f) illustrate how V_{onset} can be shifted towards more cathodic values by: (b) increasing k_{ct}, (c) reducing $k_{rec,surf}$, (d) reducing $k_{rec,bulk}$, (e) increasing V_{ph}, and (f) lowering V_{fb}.

are used in the literature to extract the value of V_{onset} from a PEC experiment. In particular, V_{onset} is often extracted from a $j(V)$ plot as: (i) the potential at which the photocurrent density exceeds a certain defined value;[129] or (ii) the potential at which the first derivative of the photocurrent density with respect to the potential, dj/dV, exceeds a certain defined value;[130] or (iii) the potential at which the tangent to the $j(V)$ curve in the region of maximum slope intersects the $j(V)$ curve measured in the dark.[131] All these definitions are somewhat arbitrary and may be more or less appropriate depending on the shape of the $j(V)$ curves to be analyzed. For instance, using method (iii) can result in a situation where a curve with a steep slope will have a more anodic V_{onset} than the one with a flatter slope, although they may have the same V_{onset} according to other methods. Thus, the choice of method to define V_{onset} may affect the exact values extracted from the $j(V)$ curves. Finally, the absolute V_{onset} value may also depend on some properties of the experimental setup, for instance the illumination intensity (on which V_{ph} depends logarithmically before saturation) and spectral distribution. Therefore, when reviewing the recent progress in the topic, we will focus here on the variation of V_{onset} rather than on their absolute values.

Accelerating the OER kinetics

The most immediate attempts to improve the performance of hematite often consist in coupling it with an electrocatalyst characterized by a higher turnover frequency. The understanding of the OER has increased significantly over the last decade thanks to the combination of detailed electrochemical characterization[132–134] with first-principles calculations[135–137] (mostly based on the density functional theory, DFT). Together with the well-known high activity for OER (and HER) of Pt,[138,139] ruthenium oxide (RuO_2), iridium oxide (IrO_2), Co and Ni based compounds have emerged as efficient catalysts.

RuO_2 and IrO_2 are both very close to the top of the volcano plot with regard to the OER activity.[137,140] While RuO_2 has already been tested as an OER co-catalyst for overall water splitting on $Ga_{1-x}Z_xN_{1-x}O_x$[141] and for the HER on CuO_2,[142] its performance as a co-catalyst for the OER on hematite is still to be investigated. However, organometallic Ru-containing complexes have recently been tested on hematite. Chen *et al.*[143] reported for instance a V_{onset} shift of about 300 mV for a hematite photoanode coated with a Ru(tpy)(pba)Cl Ru(II) complex.

IrO_2 nanoparticles on a glassy carbon support achieve an OER current of 0.5 mA cm^{-2} at an overpotential of 0.25 V.[144,145]

Table 1 Experimental approaches employed to improve the PEC properties of hematite-based photoanodes

Altered physical property	Experimental approach(es)	References
Increase k_{ct}	Overlayers	129, 143, 146, 149–152 and 154
Reduce $k_{rec,surf}$	Overlayers	39, 41, 68 and 155–164
	Post-fabrication treatments	165
Reduce $k_{rec,bulk}$	Doping	41, 96 and 166–170
	Nanostructured substrates	113 and 114
	Extra layers between Fe_2O_3 and electron collector	42 and 171–175
Increase V_{ph}	Overlayers	124 and 186
Lower V_{fb}	Post-fabrication treatments	87
	Modified fabrication	189

Tilley *et al.*[146] first attempted to couple IrO_2 to a nanocauliflower structured hematite photoanode by electrophoretic deposition. While they observed a cathodic V_{onset} shift of 200 mV, cyclic voltammetry and chronoamperometry measurements indicated a decrease in photocurrent, caused by the detachment of IrO_2 nanoparticles from the surface. The original performance could be restored by re-decorating the photoanode with additional nanoparticles. More recently, IrO_2 films were deposited on top of hematite photoanodes by means of electrodeposition, using $[Cp^*Ir\text{-}(H_2O)_3](SO_4)$ as the organometallic source of Ir.[129] A stable, maximum V_{onset} shift of 300 mV was obtained for the optimized precursor concentration (Fig. 3a). EIS revealed that the capacitance associated with surface states peaks for potentials corresponding to the OER V_{onset}, indicating that the surface states are charged with holes and then discharged when the OER is initiated. Such behavior indicates that the OER takes place *via* surface states, for this system. Mott–Schottky analysis indicated that V_{fb}, and therefore the edge of the conduction band, remains unaffected by the addition of the IrO_2 layer.

The (extreme) scarcity of both Ir and Ru poses questions on the scalability of PEC systems based on these compounds.[2] Fortunately, other OER catalysts have emerged, mainly based on first row transition metals such as Co and Ni. For example, the so-called "Co–Pi" cluster, first developed in 2008, is capable of initiating the OER at 1.7 V *vs.* RHE in a neutral environment.[147] Electrodeposition of Co–Pi films on top of hematite has been attempted, both in the dark and under illumination. After optimizing each of these two processes independently on the same dendritic photoanodes, Zhong *et al.*[148] demonstrated a V_{onset} cathodic shift of 120 and 100 mV upon photoassisted and dark electrodeposition of Co–Pi, respectively. The slightly better performance of the former method was ascribed to the more uniform deposition of the catalyst on the hematite surface, instead of the preferential deposition on pinholes for the latter one.

However, the thickness of the catalyst after optimization may be such that light absorption in the catalyst itself might compete with absorption in hematite, leading to the need for illumination from the back-side of the photoanode and thus to device design constraints. This issue was tackled for instance by Riha *et al.*,[149] who demonstrated a V_{onset} shift of 100 and 200 mV after coating planar and nanostructured hematite electrodes, respectively, with a Co-based sub-monolayer catalyst deposited by one cycle of atomic layer deposition (ALD) (Fig. 3b). The difference in V_{onset} was elucidated in terms of faster charge transfer from the surface states in modified photoanodes than from the surface states in bare electrodes, as indicated by the decreased surface state capacitance and the faster photocurrent transients observed for the coated electrodes. Moreover, XPS and XANES showed that the ALD coating consisted of 90% $Co(OH)_2$ and 10% CO_3O_4 before PEC characterization, whereas a much higher CO_3O_4 content was found after the measurements in an alkaline environment.

Ni hydroxides and oxides have also shown interesting catalytic activity towards OER. Nonetheless, a mechanistic study by Li *et al.*[150] indicated that, while photoanodes based on hematite nanowires decorated with $Ni(OH)_2$ by successive dipping into $Ni(NO_3)_2$ and NaOH solutions showed larger photocurrent during cyclic voltammetry, the steady-state photocurrent measured by chronoamperometry was smaller than in reference electrodes. The larger photocurrent response in the cyclic voltammetry experiment was understood to generate from the slow Ni^{2+}–Ni^{3+} oxidation, which eventually depletes the $Ni(OH)_2$. While cyclic voltammetry is certainly a simple, fast and often information-rich technique for preliminary evaluation of the OER photoactivity, this study shows that it is crucial to measure the steady-state photocurrent of the photoanodes (and preferably to quantify the reaction products by means of gas chromatography or mass spectrometry) in order to confirm the true photoactivity of the system.[151] More recently, Young and Hamann[152] showed a cathodic shift of V_{onset} of about 300 mV from steady state photocurrent measurements of hematite films covered by NiO by ALD. Such a result was obtained upon following a procedure developed by Trotochaud *et al.*,[153] in which the NiO-coated photoanodes were held at a constant potential of 1.42 *vs.* RHE under illumination for 3 hours. This conditioning process was determined to induce a structural change from the cubic NiO to an ion-permeable hydroxide/oxyhydroxide structure based on $Ni(OH)_2$, which was identified then as the active OER catalyst phase.

Finally, it is worth mentioning that a high activity of electrocatalysts in the dark does not always translate into improved performance when such catalysts are coupled to photoactive semiconductors. This concept was elegantly illustrated by Yang *et al.*[154] in the case of MnO_x/hematite. While MnO_x showed indeed higher OER current in the dark than hematite (both deposited in the form of thin films by ALD), addition of MnO_x onto hematite suppressed the photocurrent almost entirely. It was then hypothesized that introducing MnO_x results in Fermi level pinning, and thus in a smaller V_{ph}. Indeed, open circuit results confirmed that V_{ph} decreased from about 200 mV to 5 mV or less for the composite electrodes, indicating a clearly reduced oxidative power for holes. This result exemplifies the possibility of affecting more than one property of the photoanode by, for instance, the introduction of an additional layer.

Reducing surface recombination

Recombination of holes with electrons at the surface suppresses the photocurrent in most hematite photoanodes for moderately anodic potentials. Several attempts to alleviate this issue relied on depositing some coating (overlayer) on hematite, in a similar fashion to coupling hematite to electrocatalysts. A simple yet beneficial treatment consists in surface adsorption of Co^{2+} ions, as first attempted on hematite by Kay *et al.*[41] Treating the surface of a nanocauliflower electrode with a 10 mM $Co(NO_3)_2$ solution results in a V_{onset} shift of 80 mV, at an estimated coating thickness of just a monolayer. A very similar effect was obtained by performing the same procedure on a hematite photoanode fabricated by dip coating.[155] Although these results were first believed to originate from accelerated charge transfer kinetics, later studies have elucidated that the role of the Co^{2+} ion layer (sometimes indicated as CoO_x) is rather to reduce electron–hole recombination at the surface. Transient

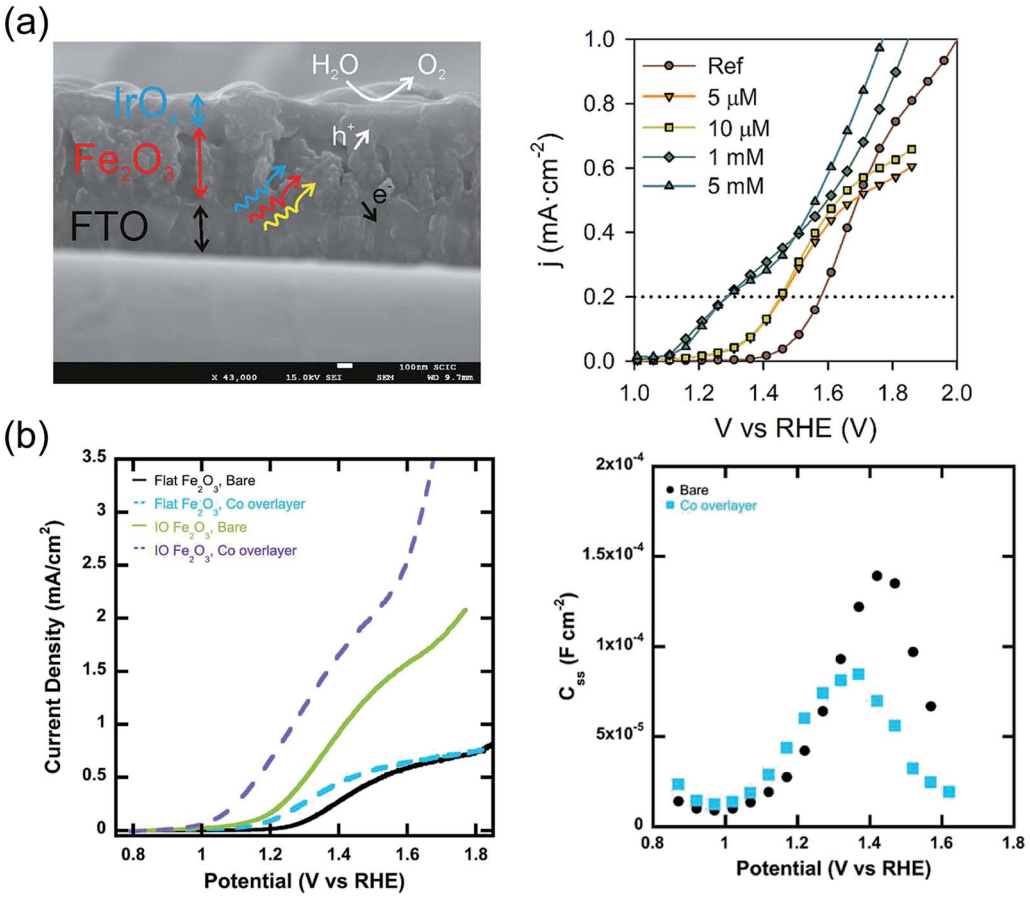

Fig. 3 (a) Left: Cross-section SEM micrograph of the FTO/hematite/IrO_2 catalyst layer. Right: $j(V)$ characteristics of hematite films covered with layers of IrO_2 with increasing thickness (right). Reproduced with permission from ref. 129. Copyright 2013 American Chemical Society. (b) Left: $j(V)$ curves for hematite films deposited on inverted opal scaffolds and covered with a Co oxide layer (left). Right: Surface states charge extracted from EIS under illumination on bare hematite and hematite after adsorption of Co oxide layer. Reproduced with permission from ref. 149. Copyright 2013 American Chemical Society.

photocurrent and transient photovoltage measurements performed on the same previously mentioned type of nanocauliflower photoelectrode, before and after Co^{2+} absorption, revealed reduced accumulated charge at the surface of the treated electrodes, as well as increased transient photovoltage.[156] These observations point at a reduced surface recombination rate $k_{rec,surf}$, and not at an increased k_{ct}. Miao *et al.*[157] drew similar conclusions on the 100 mV V_{onset} shift observed on their hydrothermally grown, Ti-doped microstructured hematite nanoparticle films, based on results from EIS measurements.

While the addition of Co–Pi layers is of proven benefit to the PEC performance of hematite, the exact mechanism of such improvement has not yet been unambiguously determined.[158] Klahr *et al.*[39] investigated the effect of Co–Pi on the photoelectrochemistry of flat hematite films grown by ALD. Transient photocurrents (Fig. 4a) indicate an increasing charging current with increasing Co–Pi thickness, which are attributed to the oxidation of Co^{3+} to Co^{4+} within the Co–Pi layer by hematite valence band holes. The EIS spectra were modeled by introducing a capacitance and charge transfer resistance associated with the Co–Pi, from which it was concluded that the latter was a fast hole-scavenger. Furthermore, MS analysis suggests that the band bending in the photoelectrode is essentially independent of the Co–Pi. In view of these results, the Co–Pi was inferred to extract photogenerated holes from hematite, thus reducing $k_{rec,surf}$. The same conclusion was drawn by Shi *et al.*,[159] who also observed a V_{onset} shift of about 220 mV upon light assisted electrodeposition of Co–Pi on hematite deposited on top of an inverse opal structured substrate.

On the other hand, Barroso and co-workers[160] have suggested a different scenario, based on their measurements on mesostructured hematite photoanodes (fabricated by APCVD or by ultrasonic spray pyrolysis) modified with Co–Pi overlayers. Transient optical absorption experiments indicated that the presence of Co–Pi induces a strong elongation of a feature centered at 700 nm, which has been assigned previously to holes generated within bulk hematite. Such transient hole decay is strongly dependent on the applied bias, and correlates well with the cathodic V_{onset} observed during cyclic voltammetry and chronoamperometry. Based on these data, the authors proposed that the Co–Pi traps electrons from hematite, and not holes, thus increasing the band bending within hematite itself. In this picture, therefore, the resulting beneficial effect would

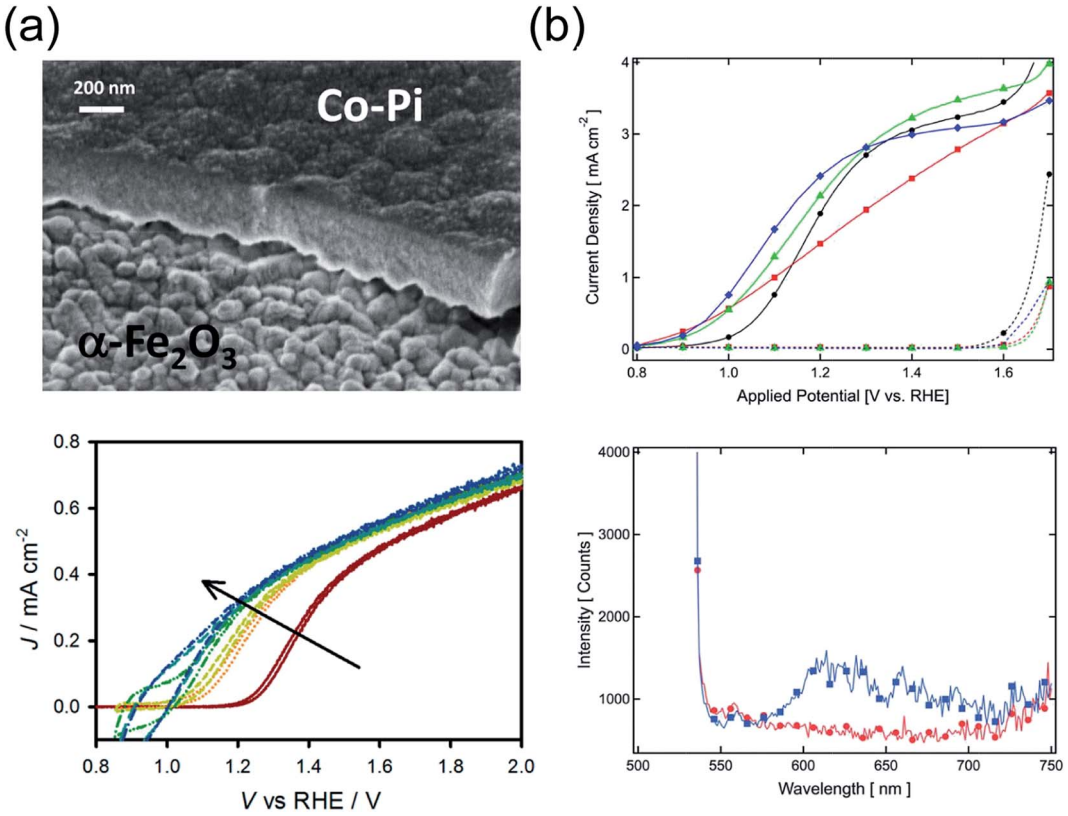

Fig. 4 (a) Cross-section SEM micrograph of hematite/Co–Pi overlayer (top), $j(V)$ curves of hematite covered with Co–Pi layers with increasing thickness (bottom). Reproduced with permission from ref. 39. Copyright 2012 American Chemical Society. (b) Top: $j(V)$ characteristics of hematite photoanodes fabricated *via* APCVD before ALD of 1 cycle of Al_2O_3 overlayer (black circles), after ALD (red squares), after annealing for 20 min at 300 °C (green triangles) and after annealing for 20 min at 400 °C (blue diamonds). Bottom: Photoluminescence emission spectra from APCVD hematite before (red circles) and after 3 ALD cycles of Al_2O_3, on its surface (blue squares). Reproduced with permission from ref. 68. Copyright 2011 The Royal Society of Chemistry.

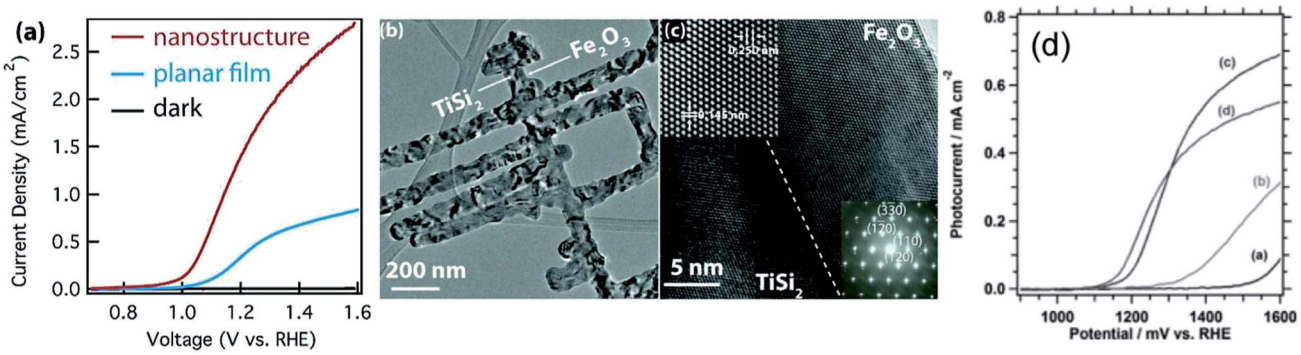

Fig. 5 (a–c) $j(V)$ plots of hematite deposited by ALD on a $TiSi_2$ nanonet substrate and of a planar hematite film; low-magnification TEM image of a typical $TiSi_2$/hematite core/shell nanostructrure; and high-resolution TEM data including lattice-fringe-resolved HRTEM image and electron diffraction pattern of hematite. Reproduced with permission from ref. 104. Copyright 2011 American Chemical Society. (d): $j(V)$ curves of 16–19 nm thick hematite deposited by USP on FTO substrates modified with different underlayers: (a) no underlayer, (b) SiO_x monolayer by TEOS spraying, (c) 2 nm thick ALD Nb_2O_5, and (d) 1 nm thick ALD TiO_2. Reproduced with permission from ref. 171. Copyright 2012 John Wiley & Sons.

be an increased charge transport in hematite thanks to reduced bulk recombination. Accordingly, there would be no transfer of holes from hematite to the Co–Pi, and the OER would still take place at the surface of hematite. These different mechanistic interpretations of the role played by Co–Pi have eventually been reconciled by Gamelin and coworkers,[161] who performed microscopic, electrochemical, and spectroscopic measurements on mesostructured Co–Pi/hematite composite photoanodes that revealed different beneficial effects of the Co–Pi layer when its thickness is changed.

Co-based coatings are not the only overlayers that have proven effective in reducing $k_{rec,surf}$. le Formal *et al.*[68] reported a

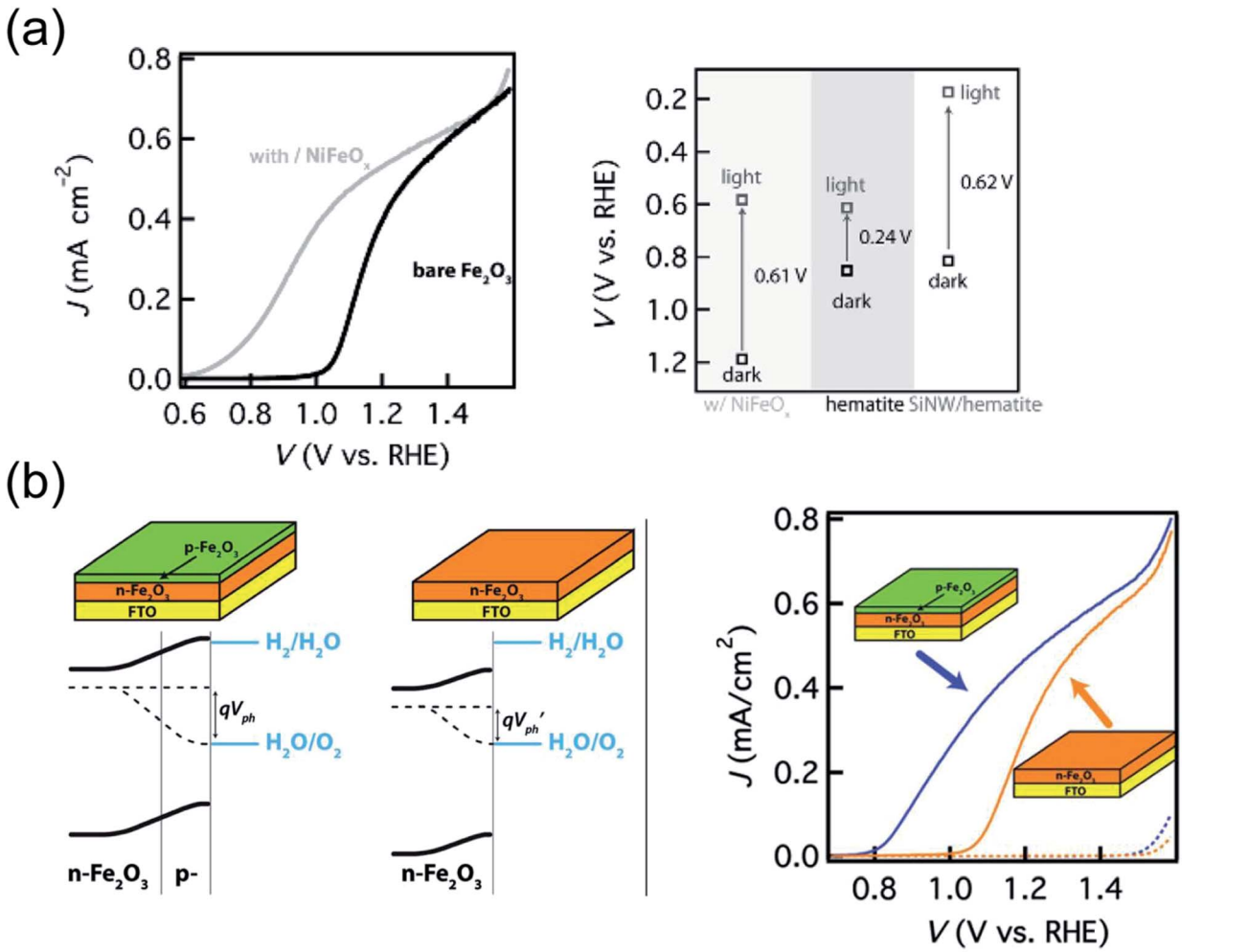

Fig. 6 (a) Left: *j*(*V*) plots of bare hematite film deposited by ALD (black) and after surface modification of hematite with $NiFeO_x$ (grey). Right: Measured V_{ph} generated by hematite decorated with $NiFeO_x$, bare hematite and hematite on Si nanowires (left, middle and right in the graph respectively). Reproduced with permission from ref. 124. Copyright 2013 The German Chemical Society. (b) Left: Energy band diagrams of unintentionally doped n-type hematite with a p-type hematite coating as compared with that of a bare n-type hematite. The presence of the p-type layer creates a built-in field that does not depend on the properties of the semiconductor/electrolyte interface, allowing an increased V_{ph}. Right: *j*(*V*) curves of n-type hematite with and without p-type coating (same total thickness of 25 nm). Reproduced with permission from ref. 186. Copyright 2012 American Chemical Society.

V_{onset} shift of 80 mV upon a one-cycle ALD coating of nanostructured hematite photoanodes with Al_2O_3. Thicknesses of up to 13 cycles of Al_2O_3 were tested, showing a similar beneficial effect in terms of V_{onset} shift. However, the coatings dissolved after 1 h chronoamperometry under 1 sun illumination at 1.05 V *vs.* RHE. Transient photocurrent measurements and EIS indicated a lower surface recombination rate while the position of the band edges in hematite was unaffected. Finally, photoluminescence at wavelengths between 600 and 700 nm was observed in Al_2O_3-coated photoelectrodes, pointing at a passivating effect of the overlayer on the surface states (the OER was found here to take place *via* direct transfer of holes from the valence band) (Fig. 4b).

Spurred by these observations, Hisatomi and coworkers[162] undertook a systematic screening of the effect of 13-group oxide overlayers on the photoelectrochemistry of hematite ultra-thin films fabricated by USP. The coatings, consisting of Al_2O_3, Ga_2O_3, or In_2O_3, were prepared by chemical bath deposition based on urea hydrolysis. The highest V_{onset} shift of 200 mV was obtained with a Ga_2O_3 coating after calcination at 500 °C. The after-deposition thermal treatment also helped preventing dissolution of the overlayer for about one day. The superior performance of Ga_2O_3 as compared to the other coatings was rationalized in terms of the ability of Ga_2O_3 (which has the smallest lattice mismatch with hematite) to release lattice strain of the thin hematite layers.

Besides 13-group oxide overlayers, Xi and coworkers[163] demonstrated a 170 mV cathodic V_{onset} shift on hematite films fabricated by spray pyrolysis upon coating with a ZnO layer deposited by spin-coating a zinc acetate solution in ethanol and subsequent calcination at 400 °C. An optimal number of 3 cycles was found, resulting in a ZnO thickness of a few nm as estimated by XPS. The beneficial effect of the surface treatment in terms of suppressing surface recombination was assessed by

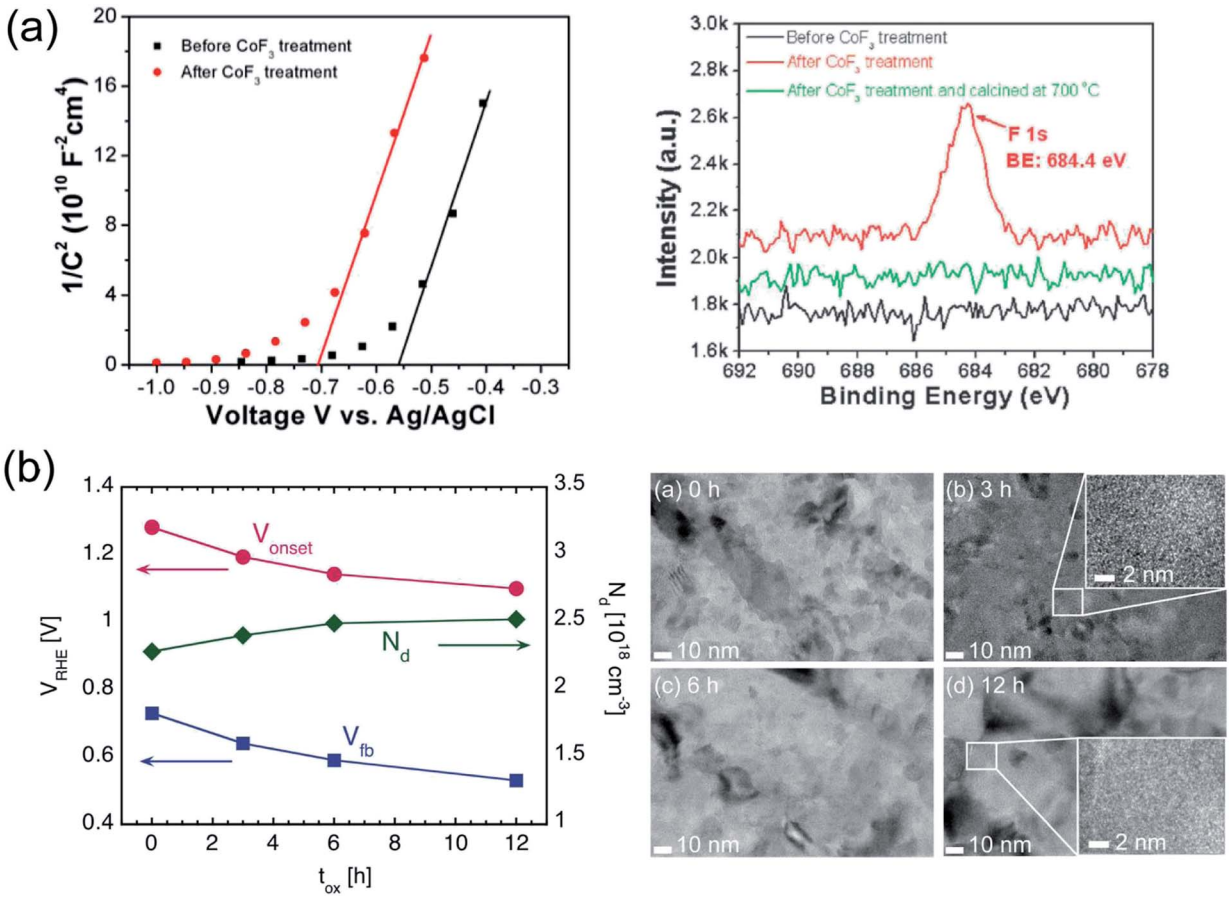

Fig. 7 (a) Left: MS plots for electrodeposited hematite films before and after treatment in solution containing CoF_3. Right: F 1s high-resolution XPS spectra of Ti-doped hematite film, Ti-doped hematite film after CoF_3 aqueous solution treatment without and with high temperature calcination. Reproduced with permission from ref. 87. Copyright 2009 The Royal Society of Chemistry. (b) Left: V_{onset} and V_{fb} of ultrathin hematite films fabricated by thermal oxidation of Fe, as a function of oxidation time. The majority charge carrier concentration N_D is also plotted. Right: TEM images of hematite films held at 350 °C during thermal conversion for 0, 3, 6 and 12 h. High magnification insets are also present for 3 and 12 h samples. From ref. 189.

extracting the ideality factor from current–potential measurements performed in the dark under forward bias. A shift of V_{fb} towards lower values of about 35 mV was determined from MS plots, which may also have partly contributed to the observed V_{onset} shift. The same group modified a route to incorporate a thin coating of $Fe_xSn_{1-x}O_4$ on the surface of hydrothermally grown FeOOH nanowires.[164] The thickness of the amorphous $Fe_xSn_{1-x}O_4$ was determined to be 1–2 nm by high resolution TEM imaging. Chopped chronoamperometry and ideality factor measurements in the dark both supported the claim that $Fe_xSn_{1-x}O_4$ improves the delivery of holes to the electrolyte by decreasing $k_{rec,surf}$.

Finally, further post-fabrication treatments have proven to decrease $k_{rec,surf}$. For instance, Zhang *et al.*[165] demonstrated a V_{onset} shift of about 200 mV for hematite films fabricated by USP, after prolonged chronoamperometry in a saturated NaCl electrolyte under illumination of intensity of *ca.* 400 mW cm^{-2}. Dissolution of the outermost layers of the hematite films during this treatment was inferred from inductively coupled plasma mass spectrometry analysis. Photocurrent transients were found to be less pronounced for treated electrodes, which, coupled with an increase in the photoluminescence signal centered around 610 nm, indicated a beneficial effect of the treatment on the hole transfer efficiency across the hematite/electrolyte interface.

Improving carrier transport in bulk

The most common strategy to alleviate the issue of bulk recombination consists in doping hematite. Perhaps the most emphasized result of incorporating foreign atoms is the enhanced maximum photocurrent j_{max}. Nevertheless, a V_{onset} shift is also often observed, due to the fact that for moderately anodic potentials not only η_{ct}, but also η_{tr} is far from unity. A beneficial effect of doping on V_{onset} is mentioned in some reports, and can originate from the enhanced conductivity thanks to the increase in charge donors, from the improved morphology of hematite, or from both.

For instance, Cao *et al.*[166] showed a V_{onset} shift of about 100 mV on hematite films grown *via* hydrothermal reaction upon Ti doping during fabrication. While the doped samples did not show any appreciable difference from reference electrodes in

terms of surface structure, morphology and radiative recombination by photoluminescence, a clear increase in the donor concentration was determined from doping with Ti^{4+}, which accounted for the improved PEC performance. Cong and coworkers[167] reported a beneficial synergistic effect of Al and Ta co-doping of hematite films grown by drop casting and subsequent annealing. While Al^{3+} incorporation in hematite does not increase the charge carrier density, its smaller ionic radius as compared to Fe^{3+} was shown to facilitate charge hopping through the semiconductor. Ta^{5+} ions, instead, enhance the conductivity in a similar fashion to Ti^{4+} and Si^{4+} dopants. Optimized 0.25% Ta/10% Al co-doped hematite films showed a V_{onset} more than 200 mV more cathodic than 10% Al only doped electrodes, even though V_{fb} was determined to be higher by 50 mV in the former case. EIS under illumination revealed a drastically reduced resistance for the co-doped electrodes, corroborating the hypothesis of reduced bulk recombination.

Coupling of hematite photoanodes with carbon nanotubes has also been explored recently. Kim *et al.*[168] found an anodic V_{onset} shift of about 50 mV on a multi-walled carbon nanotubes/hematite composite electrode, where the hematite films were fabricated by calcination of Fe nanoparticle films. On the other hand, they observed a beneficial effect of the nanotubes on j_{max}, which increased by a factor of about 3 thanks to the enhanced bulk conductivity as confirmed by EIS characterization. Liu and coworkers,[96] instead, found a cathodic V_{onset} shift of 140 mV upon functionalization of Ti-doped electrodeposited hematite films with carbon nanotubes, which were dispersed in the electrodeposition solution prior to fabrication. A combination of transient photocurrent and EIS measurements was employed to support the hypothesis that the carbon nanotubes work as an efficient electron sink, thus reducing electron–hole recombination in the bulk.

Doping of hematite can also be accomplished as post-fabrication treatment, as demonstrated by Franking and coworkers,[169] who developed a method to dope hematite nanowire films by depositing a doping precursor solution (Ti or Zr) with subsequent annealing at 650–700 °C. A 50 mV V_{onset} shift was found after 30 minutes annealing of the films after modification with the Ti-containing precursor. The enhanced PEC performance was attributed to the one order of magnitude increase in charge carrier density, as determined by MS analysis. Interaction of the dopant atoms with surface states in hematite, however, was inferred from EIS under illumination, and could also play a role in the superior performance of the treated photoanodes.

The influence of doping on the morphology of hematite is perhaps best exemplified by the results reported by Kay *et al.*[41] in 2006, which demonstrated for the first time dendritic, cauliflower-like nanostructured hematite with a strong preferential orientation of the [110] axis vertical to the substrate induced by Si^{4+} doping. Photoanodes fabricated through the same APCVD technique are still the benchmark for the OER on hematite. More recently, Lee and coworkers showed that Si doping of hematite nanotubes resulted in more pronounced nanotubular morphology than for unintentionally doped samples.[170] Although XRD analysis did not show a drastic improvement in crystallinity, the increased surface area of the Si doped electrodes resulted in an appreciable V_{onset} shift of around 160 mV.

Depositing hematite on nanostructured templates has proven to be an effective means to increase η_{tr}, and therefore improving the PEC performance at low applied bias. Riha *et al.*[113] employed a simple fabrication protocol to deposit hematite by ALD on top of a porous inverse opal scaffold substrate. These nanostructured electrodes showed a 200 mV V_{onset} shift as well as a 3-fold increase of j_{max} at 1.53 *vs.* RHE as compared to flat ITO/hematite films. Along the same line, Lin and coworkers[104] realized nanostructured hematite photoanodes by conformal ALD coating of high conductivity, highly crystalline $TiSi_2$ nanonets constituting of belts about 1–2 μm long and around 15 nm in diameter (Fig. 5a–c). These nanonets served as both a substrate support and an electron collector, thus providing an interesting alternative to transparent conductive oxides. The bulk recombination was dramatically reduced as compared to planar film geometry, leading to a cathodic V_{onset} shift of around 150 mV as well as an enhancement of j_{max} by a factor of five. While in both these reports ALD is used to cover the nanostructured substrate in a conformal way with low defect concentration hematite, this approach may be extended by doping the hematite and by depositing it *via* more easily scalable techniques.

A common denominator in the poor η_{tr} observed for many hematite based photoanodes is charge recombination at the solid/solid interface between hematite and the electron collection layer. This issue can be alleviated by introducing an additional layer between the charge collector and the hematite, which has a proper conduction band edge position in order to mitigate the recombination at the back of the electrode. Hisatomi and coworkers[171] first investigated the effect of ALD fabricated Nb_2O_5 and TiO_2 underlayers on the PEC properties of ultra-thin hematite deposited by USP (Fig. 5d). When deposited directly on FTO, hematite films of thickness lower than 20 nm showed negligible photocurrent, while they started the OER at around 1.1 V *vs.* RHE and reached j_{max} between 0.6 and 0.7 mA cm^{-2} upon introduction of a Nb_2O_5 or TiO_2 underlayer. The photocurrent decreased with increasing thickness of the TiO_2 underlayer, which was explained by the need for electrons to tunnel through the underlayer to reach the FTO due to the high offset of 0.6 eV between the conduction band edges of TiO_2 and hematite. On the other hand, thanks to the lower offset in the case of Nb_2O_5/hematite (only 0.2 eV), the photocurrent increased with increasing Nb_2O_5 thickness (at constant V_{onset}), stabilizing at a thickness of 1.5 nm. The most convincing evidence that the performance improvement originated from the suppression of back injection of electrons came from the drastic reduction in cathodic dark current measured in the presence of the fast $Fe(II)(CN)_6^{4-}/Fe(III)(CN)_6^{3-}$ redox couple. A very similar trend was observed by Wang *et al.*[172] for TiO_2 underlayers between FTO and comparatively thicker (100 nm) hematite films deposited by the same USP. In this case the underlayer was obtained by a layer-by-layer exfoliation from titanium oxide nanosheets followed by calcination. The authors also found an optimal thickness of the underlayer, given by 2

nanosheet deposition cycles, corresponding to 1.46 nm in excellent agreement with the previous report.

A variety of further underlayers have been tested recently with similar promising results. Meng and coworkers[173] prepared composite reduced graphene oxide/hematite photoanodes. The superior performance of the composite photoanodes was established by cyclic voltammetry, transient photocurrent and TAS measurements, showing a V_{onset} shift of about 200 mV compared to bare hematite samples. Yang and coworkers[174] demonstrated a cathodic V_{onset} shift of almost 100 mV by introducing an unintentionally doped hematite underlayer between the FTO substrate and Ti-doped nanowire hematite films. The beneficial effect was explained in terms of suppression of back injection of electrons thanks to the lower conductivity of the unintentionally doped underlayer as compared to the Ti-doped nanowires.

The introduction of other oxide layers between the charge collector and hematite often provides a template for growth of hematite of higher quality in terms of reduced growth stress, improved crystallinity or improved morphology. le Formal and coworkers[175] showed that pretreating FTO substrates with tetraethoxysilicate (TEOS) prior to deposition of hematite by USP resulted in a V_{onset} shift of 70 mV for 23 nm thick hematite films. Detailed physical characterization of these ultra-thin films revealed that the pretreatment resulted in the formation of a monolayer of SiO_x on the substrate. The subsequently deposited hematite films showed increased crystallinity and reduced defects acting as trapping states, as determined by XRD and transient photocurrent measurements. It was suggested that such differences arise from different film formation processes: a Frank–van der Merwe growth (*i.e.* full layer covering the substrate) and a Volmer–Weber growth mode (*i.e.* film formation by islands) on SiO_x modified and bare FTO substrate respectively. Similar results were obtained by Hisatomi *et al.*[42] using a Ga_2O_3 underlayer deposited by ALD prior to deposition of ultra-thin hematite films by USP. After optimization of the thickness of the underlayer, a V_{onset} shift of 200 mV was demonstrated. Based on investigation of the morphology and crystallinity by SEM and XRD respectively, it was asserted that the underlayer works as an isostructural template for the hematite growth.

Finally, several further studies have demonstrated the beneficial effect of improved quality of hematite on the bulk recombination.[85,105,173–185] The schemes explored to obtain such performance improvement include: coating with suitable overlayers, co-sputtering of other oxides with hematite to obtain solid oxide solutions, tuning fabrication parameters or optimizing the post-fabrication annealing conditions.

Increasing photovoltage

As described in the Introduction, the difference between quasi-Fermi levels for electrons and holes ($E_{F,n}$ and $E_{F,p}$ respectively) determines the photovoltage V_{ph} in the semiconductor. The latter can in principle approach the optical bandgap, however this is far from being the case for hematite in practice. The magnitude of V_{ph} is normally determined by measuring the difference between open circuit potential, OCP (*i.e.* when no net current flow is present at the semiconductor/electrolyte interface) in the dark and under illumination. At equilibrium in the dark, the OCP reports on the position of the Fermi level, *i.e.* $E_{F,n} = E_{F,p} = E_F$. Under illumination, the equilibrium between the photoelectrode and electrolyte is instead maintained by $E_{F,p}$. Therefore, the difference between the OCP measured in the two situations corresponds to the V_{ph}. The latter is often 0.2–0.3 eV for hematite,[124] highlighting the potential room for improvement. However, it was not until very recently that strategies to increase V_{ph}, and thus the driving force of holes towards the OER, were demonstrated.

In the first case, Du *et al.*[124] reported a V_{onset} shift as high as 380 mV upon decorating hematite films with an amorphous $NiFeO_x$ layer, prepared by photochemical metal–organic deposition (Fig. 6a). While $NiFeO_x$ was recently identified as an efficient OER catalyst in the dark, its beneficial effect on the photoelectrochemistry of hematite was rationalized as originating from an increase of V_{ph} rather than an acceleration of k_{ct}. In fact, while the open circuit potential under illumination was practically unmodified by the presence of $NiFeO_x$, the open circuit potential in the dark shifted from 0.85 V in the case of bare hematite to 1.23 V after modification. Such a difference of 380 mV arises from removal of the surface states pinning at the hematite/electrolyte junction, and accounts for the observed V_{onset} shift.

In the second case, 5 nm thick, p-type Mg-doped hematite was grown on n-type (due to oxygen vacancies) hematite films.[186] TEM imaging revealed that the growth of p-type hematite does not introduce additional structural defects. Cyclic voltammetry indicated a 200 mV shift of V_{onset} upon deposition of the p-type hematite coating (Fig. 6b). The presence of the additional in-built field leading to the increase in V_{ph} was confirmed by EIS performed in the dark as well as by transient V_{ph} measurements, which demonstrated that the buried p–n junction acts as a favorable charge recombination center when light is switched off. Moreover, changes in optical absorption and in film thickness were ruled out as possible parameters influencing the difference in PEC performance, while a MgO coating on hematite control films did not show any V_{onset} shift thus excluding the possibility that the p-type coating reduces charge recombination at the surface.

Shifting the flat band potential

Another interesting, yet largely unexplored strategy to lower V_{onset} consists in lowering V_{fb} in hematite. If this goal is accomplished, the potential at which the bands in the semiconductor start bending upwards, thus driving holes toward the semiconductor/electrolyte interface, is also lowered. The same effect can be explained in that, for a given value of applied potential, the width of the depletion layer W_{SC} is increased since W_{SC} typically scales with $(V - V_{fb})^{0.5}$. Lowering V_{fb} is therefore desirable since it would lead to a lowering of V_{onset} as well, provided that the other PEC properties of the system remain unmodified. A modification of V_{fb} resulting in enhanced TiO_2 based photocatalysis has been demonstrated, for instance by

tuning the level of oxygen vacancies.[187,188] Recently, a similar effect has also been reported for hematite-based PEC devices.[87,163,189]

Part of the V_{onset} shift observed by Xi *et al.*[163] upon modification of hematite with a ZnO overlayer was explained by a lowering of V_{fb} of 35 mV. A more substantial V_{fb} shift was demonstrated by Hu and coworkers[87] on a system consisting of a Ti-doped hematite film fabricated by electrodeposition, which was treated with a CoF_3 solution (Fig. 7a). XPS depth analysis indicated that the surface of the Ti-doped samples is enriched with Ti relative to the bulk of the film, which facilitates the grafting of F^- ions to the surface due to the more favorable Gibbs free energy of $TiFe_3$ formation as compared to FeF_3. Photoelectrodes treated with the CoF_3 solution showed a cathodic V_{onset} shift of 200 mV as compared to untreated samples. A V_{fb} shift of 170 mV was determined from MS analysis, which accounted for the beneficial effect on V_{onset}.

It is also possible to lower V_{fb} in hematite without additional layers or other post-fabrication treatments.[189] A lowering of V_{fb} of 200 mV on polycrystalline ultra-thin hematite films was achieved by prolonging the oxidation process during which the Fe films were converted into hematite (Fig. 7b). An excellent agreement between the shift of V_{fb} extracted from MS analysis and that of V_{onset} observed during photocurrent measurements was found, while the plateau photocurrent only increased by about 10%. Optical absorption, surface composition, density of surface states and roughness were all unaffected by the prolonged oxidation. TEM analysis, instead, revealed an increase in grain size (and thus decreasing grain boundary density) for increasing oxidation time that correlated qualitatively with the observed V_{fb}, in terms of reduced potential losses at boundaries within the hematite.

Conclusions

Decades of research on the PEC properties of hematite have identified a number of specific limitations that have prevented us so far from achieving the theoretical maximum STH conversion efficiency of this material. Nevertheless, the favorable characteristics of hematite in terms of bandgap energy, exceptional stability and availability make it one of the most promising candidates for solar energy storage. Here we have analyzed in detail a major issue that needs to be solved in order to make hematite suitable for large-scale applications, namely the highly anodic electrochemical potential required to initiate the OER. We now understand this to be the result of a combination of several factors and properties, both of hematite and of the hematite/electrolyte interface: a slow OER kinetics, often much slower than charge recombination at the hematite/electrolyte interface; bulk losses arising from charge recombination within hematite; a small V_{ph} compared to the optical bandgap, resulting in a low oxidative power of holes; and an often high value of V_{fb}.

We have summarized the recent advancements in lowering V_{onset}, which in most cases focus on improving one of the aforementioned processes/properties (OER kinetics, surface recombination, bulk recombination, photovoltage and flat band potential) at the time. Several experimental strategies have proven effective, and some of them demonstrated remarkable improvements, with measured V_{onset} shifts of up to 0.4 V as compared to reference samples without modifications. Moreover, many of these approaches are (in principle) compatible with one another, for instance doping of hematite with underlayers and/or (catalyst) overlayers. Indeed, hematite based composite photoanodes that incorporate different modifications have been successfully fabricated. Nonetheless, the performance of such modified photoelectrodes is still quite far from what can be achieved using hematite, with an ideal performance of $V_{onset} = V_{fb} = 0.4$–0.5 V and a $j_{max} = 12$ mA cm^{-2} reached within 0.1 V of V_{onset}. A further motivation to push the performance of hematite consists in that reaching j_{max} at 0.7 V or lower potential would allow for using one single-junction Si-based PV device in series with the photoanode, to provide all the necessary bias to run the OER.

The following considerations can be made to rationalize the performance gap in hematite. First, the majority of the studies presented here are characterized by the use of model photoelectrodes, and in general by photoelectrodes whose performance is far from state-of-the-art. While these studies are undoubtedly important as proof-of-principle for new avenues for improvement and as platforms for increasing material understanding, it is indeed questionable whether the beneficial effect would be translated quantitatively to state-of-the-art photoelectrodes. Second, a few modifications of hematite have been shown to affect more than one property of the system, and not always in a beneficial way. In some cases, the overall performance of the photoanodes was even worsened as compared to unmodified samples. Third (and in relation to the previous point), when attempting to combine different modification strategies, the total V_{onset} shift is likely not given by the sum of the shifts seen for each modification alone, or in other words saturation of the performance improvement can be expected.

Clearly, there is plenty of room to improve both the kinetics of the OER and the energetics of the hematite/electrolyte junction. Moreover, the requirement of cheap and scalable fabrication calls for the use of deposition techniques yielding films characterized by significantly poorer quality (crystallinity, density of defects and so on) than for instance single crystal films, which calls for improving the properties of these photoelectrodes with (some of) the modifications discussed here. It is safe to assume that several of these approaches need to be combined in order to reach the goals described above, *i.e.* $V_{onset} = V_{fb} = 0.4$–0.5 V and a $j_{max} = 12$ mA cm^{-2} reached within 0.1 V of V_{onset}.

Doping (by foreign atoms or by tuning the amount of oxygen vacancies) is required to enhance electron conductivity, while the presence of an extra layer between hematite and the electron collector is the key to reduce the back-injection of electrons into hematite. These two strategies combined carry the promise of solving the issue of internal charge recombination. Furthermore, the addition of overlayers is paramount to accelerate the notoriously slow OER kinetics on hematite, as well as to increase the photovoltage sustained by the electrode. The

question remains, however, whether these modifications are compatible with one another in practice: for instance, when some of them require heat treatment at temperatures that cannot be sustained by certain catalysts. Nevertheless, besides the remarkable advancements in hematite based water splitting over the last decade, the massive effort summarized here is crucial since it has enabled the PEC community to deepen the understanding of the properties of hematite tremendously. We consider this to be a key ingredient in designing photoanodes that will take advantage of the full potential of hematite.

Acknowledgements

B. I. and A. H. thank the Swedish Research Council, Formas (project numbers 219-2011-959 and 229-2009-772) and the Chalmers Area of Advance Material and Energy for financial support. B. W. thanks Formas (project number 219-2011-959) for financial support. I. Z. acknowledges support from the Swedish Pension Agency.

References

1 *BP Statistical Review of World Energy*, 2011, http://www.bp.com/en/global/corporate/about-bp/energy-economics/statistical-review-of-world-energy.html.
2 P. C. K. Vesborg and T. F. Jaramillo, *RSC Adv.*, 2012, **2**, 7933.
3 N. S. Lewis and D. G. Nocera, *Proc. Natl. Acad. Sci. U. S. A.*, 2006, **103**, 15729–15735.
4 N. Armaroli and V. Balzani, *Angew. Chem., Int. Ed. Engl.*, 2007, **46**, 52–66.
5 R. E. Smalley, *MRS Bull.*, 2011, **30**, 412–417.
6 K. Rajeshwar, R. McConnell, K. Harrison and S. Licht, in *Solar Hydrogen Generation – toward a Renewable Energy Future*, Springer, New York, 2008.
7 J. Barber, *Philos. Trans. R. Soc., A*, 2007, **365**, 1007–1023.
8 J. Turner, G. Sverdrup, M. K. Mann, P.-C. Maness, B. Kroposki, M. Ghirardi, R. J. Evans and D. Blake, *Int. J. Energy Res.*, 2008, **32**, 379–407.
9 D. Gust, T. A. Moore and A. L. Moore, *Faraday Discuss.*, 2012, **155**, 9.
10 C. A. Grimes, O. K. Varghese and S. Ranjan, *Light, Water, Hydrogen*, Springer, 2008.
11 Ed. R. van de Krol and M. Grätzel, *Photoelectrochemical Hydrogen Production*, Springer, US, Boston, MA, 2012, vol. 102.
12 P. J. Boddy, *J. Electrochem. Soc.*, 1968, **115**, 199.
13 A. Fujishima and K. Honda, *Nature*, 1972, **238**, 37–38.
14 M. Grätzel, *Nature*, 2001, **414**, 338–344.
15 F. E. Osterloh, *Chem. Mater.*, 2008, **20**, 35–54.
16 M. Woodhouse and B. A. Parkinson, *Chem. Soc. Rev.*, 2009, **38**, 197–210.
17 J. Greeley, T. F. Jaramillo, J. Bonde, I. B. Chorkendorff and J. K. Nørskov, *Nat. Mater.*, 2006, **5**, 909–913.
18 A. Walsh, S.-H. Wei, Y. Yan, M. Al-Jassim, J. Turner, M. Woodhouse and B. Parkinson, *Phys. Rev. B: Condens. Matter Mater. Phys.*, 2007, **76**, 165119.
19 O. Khaselev and J. A. Turner, *Science*, 1998, **280**, 425–427.
20 A. Fujishima, X. Zhang and D. Tryk, *Surf. Sci. Rep.*, 2008, **63**, 515–582.
21 M. Ni, M. K. H. Leung, D. Y. C. Leung and K. Sumathy, *Renewable Sustainable Energy Rev.*, 2007, **11**, 401–425.
22 J. Yu, L. Qi and M. Jaroniec, *J. Phys. Chem. C*, 2010, **114**, 13118–13125.
23 I. S. Cho, C. H. Lee, Y. Feng, M. Logar, P. M. Rao, L. Cai, D. R. Kim, R. Sinclair and X. Zheng, *Nat. Commun.*, 2013, **4**, 1723.
24 G. Wang, H. Wang, Y. Ling, Y. Tang, X. Yang, R. C. Fitzmorris, C. Wang, J. Z. Zhang and Y. Li, *Nano Lett.*, 2011, **11**, 3026–3033.
25 N. Gaillard, Y. Chang, J. Kaneshiro, A. Deangelis and E. L. Miller, *Proc. SPIE*, 2010, **7770**, 77700V, DOI: 10.1117/12.860970.
26 M. Huda, Y. Yan, C.-Y. Moon, S.-H. Wei and M. Al-Jassim, *Phys. Rev. B: Condens. Matter Mater. Phys.*, 2008, **77**, 195102.
27 B. Cole, B. Marsen, E. Miller, Y. Yan, B. To, K. Jones and M. Al-Jassim, *J. Phys. Chem. C*, 2008, **112**, 5213–5220.
28 M. Bär, L. Weinhardt, B. Marsen, B. Cole, N. Gaillard, E. Miller and C. Heske, *Appl. Phys. Lett.*, 2010, **96**, 032107.
29 A. Tacca, L. Meda, G. Marra, A. Savoini, S. Caramori, V. Cristino, C. A. Bignozzi, V. Gonzalez Pedro, P. P. Boix, S. Gimenez and J. Bisquert, *ChemPhysChem*, 2012, **13**, 3025–3034.
30 X. Yang, A. Wolcott, G. Wang, A. Sobo, R. C. Fitzmorris, F. Qian, J. Z. Zhang and Y. Li, *Nano Lett.*, 2009, **9**, 2331–2336.
31 S. Shet, *ECS Trans.*, 2011, **33**(38), 15–25.
32 Y. Wei, L. Ke, J. Kong, H. Liu, Z. Jiao, X. Lu, H. Du and X. W. Sun, *Nanotechnology*, 2012, **23**, 235401.
33 A. Wolcott, W. A. Smith, T. R. Kuykendall, Y. Zhao and J. Z. Zhang, *Adv. Funct. Mater.*, 2009, **19**, 1849–1856.
34 Y. Park, K. J. McDonald and K.-S. Choi, *Chem. Soc. Rev.*, 2013, **42**, 2321–2337.
35 B. Xie, H. Zhang, P. Cai, R. Qiu and Y. Xiong, *Chemosphere*, 2006, **63**, 956–963.
36 F. F. Abdi and R. van de Krol, *J. Phys. Chem. C*, 2012, **116**, 9398–9404.
37 Y. Liang, T. Tsubota, L. P. A. Mooij and R. van de Krol, *J. Phys. Chem. C*, 2011, **115**, 17594–17598.
38 S. P. Berglund, A. J. E. Rettie, S. Hoang and C. B. Mullins, *Phys. Chem. Chem. Phys.*, 2012, **14**, 7065–7075.
39 B. Klahr, S. Gimenez, F. Fabregat-Santiago, J. Bisquert and T. W. Hamann, *J. Am. Chem. Soc.*, 2012, **134**, 16693–16700.
40 N. Beermann, L. Vayssieres, S.-E. Lindquist and A. Hagfeldt, *J. Electrochem. Soc.*, 2000, **147**, 2456.
41 A. Kay, I. Cesar and M. Grätzel, *J. Am. Chem. Soc.*, 2006, **128**, 15714–15721.
42 T. Hisatomi, J. Brillet, M. Cornuz, F. le Formal, N. Tétreault, K. Sivula and M. Grätzel, *Faraday Discuss.*, 2012, **155**, 223.
43 H. Dotan, O. Kfir, E. Sharlin, O. Blank, M. Gross, I. Dumchin, G. Ankonina and A. Rothschild, *Nat. Mater.*, 2013, **12**, 158–164.
44 A. B. Murphy, P. R. F. Barnes, L. K. Randeniya, I. C. Plumb, I. E. Grey, M. D. Horne and J. A. Glasscock, *Int. J. Hydrogen Energy*, 2006, **31**, 1999–2017.

45 J. Brillet, J.-H. Yum, M. Cornuz, T. Hisatomi, R. Solarska, J. Augustynski, M. Graetzel and K. Sivula, *Nat. Photonics*, 2012, **6**, 824–828.
46 K. L. Hardee, *J. Electrochem. Soc.*, 1976, **123**, 1024.
47 L. A. Marusak, R. Messier and W. B. White, *J. Phys. Chem. Solids*, 1980, **41**, 981–984.
48 L.-S. R. Yeh, *J. Electrochem. Soc.*, 1977, **124**, 833.
49 G. Ketteler, W. Weiss, W. Ranke and R. Schlögl, *Phys. Chem. Chem. Phys.*, 2001, **3**, 1114–1122.
50 R. M. Cornell and U. Schwertmann, *The Iron Oxides*, Wiley-VCH Verlag GmbH & Co. KGaA, Weinheim, FRG, 2003.
51 K. Sivula, F. le Formal and M. Grätzel, *ChemSusChem*, 2011, **4**, 432–449.
52 K. M. H. Young, B. M. Klahr, O. Zandi and T. W. Hamann, *Catal. Sci. Technol.*, 2013, **3**, 1660.
53 M. J. Katz, S. C. Riha, N. C. Jeong, A. B. F. Martinson, O. K. Farha and J. T. Hupp, *Coord. Chem. Rev.*, 2012, **256**, 2521–2529.
54 J. Tauc, *Mater. Res. Bull.*, 1968, **3**, 37–46.
55 I. Balberg and H. L. Pinch, *J. Magn. Magn. Mater.*, 1978, **7**, 12–15.
56 N. F. Mott and R. Peierls, *Proc. Phys. Soc., London*, 1937, **49**, 72–73.
57 P. Liao, M. C. Toroker and E. A. Carter, *Nano Lett.*, 2011, **11**, 1775–1781.
58 P. Liao and E. A. Carter, *J. Appl. Phys.*, 2012, **112**, 013701.
59 A. J. Bosman and H. J. van Daal, *Adv. Phys.*, 1970, **19**, 1–117.
60 R. Chang and J. Wagner Jr, *J. Am. Ceram. Soc.*, 1972, 211–213.
61 T. Nakau, *J. Phys. Soc. Jpn.*, 1960, **15**, 727.
62 D. Benjelloun, J.-P. Bonnet, J.-P. Doumerc, J.-C. Launay, M. Onillon and P. Hagenmuller, *Mater. Chem. Phys.*, 1984, **10**, 503–518.
63 K. M. Rosso, D. M. A. Smith and M. Dupuis, *J. Chem. Phys.*, 2003, **118**, 6455.
64 N. J. Cherepy, D. B. Liston, J. A. Lovejoy, H. Deng and J. Z. Zhang, *J. Phys. Chem. B*, 1998, **102**, 770–776.
65 A. G. Joly, J. R. Williams, S. A. Chambers, G. Xiong, W. P. Hess and D. M. Laman, *J. Appl. Phys.*, 2006, **99**, 053521.
66 F. Morin, *Phys. Rev.*, 1954, **93**, 1195–1199.
67 M. Sastri and G. Nagasubramanian, *Int. J. Hydrogen Energy*, 1982, **7**, 873–876.
68 F. le Formal, N. Tétreault, M. Cornuz, T. Moehl, M. Grätzel and K. Sivula, *Chem. Sci.*, 2011, **2**, 737.
69 F. le Formal, S. R. Pendlebury, M. Cornuz, S. D. Tilley, M. Grätzel and J. R. Durrant, *J. Am. Chem. Soc.*, 2014, **136**, 2564–2574.
70 A. Hellman and R. G. S. Pala, *J. Phys. Chem. C*, 2011, **115**, 12901–12907.
71 X.-G. Wang, W. Weiss, S. Shaikhutdinov, M. Ritter, M. Petersen, F. Wagner, R. Schlögl and M. Scheffler, *Phys. Rev. Lett.*, 1998, **81**, 1038–1041.
72 S. Yin, X. Ma and D. E. Ellis, *Surf. Sci.*, 2007, **601**, 2426–2437.
73 T. P. Trainor, A. M. Chaka, P. J. Eng, M. Newville, G. A. Waychunas, J. G. Catalano and G. E. Brown, *Surf. Sci.*, 2004, **573**, 204–224.
74 L. M. Peter, K. G. U. Wijayantha and A. A. Tahir, *Faraday Discuss.*, 2012, **155**, 309.
75 B. Klahr, S. Gimenez, F. Fabregat-Santiago, J. Bisquert and T. W. Hamann, *Energy Environ. Sci.*, 2012, **5**, 7626.
76 K. G. Upul Wijayantha, S. Saremi-Yarahmadi and L. M. Peter, *Phys. Chem. Chem. Phys.*, 2011, **13**, 5264–5270.
77 L. M. Peter, K. G. U. Wijayantha and A. A. Tahir, *Faraday Discuss.*, 2012, **155**, 309.
78 C. Y. Cummings, F. Marken, L. M. Peter, A. A. Tahir and K. G. U. Wijayantha, *Chem. Commun.*, 2012, **48**, 2027–2029.
79 C. Y. Cummings, F. Marken, L. M. Peter, K. G. U. Wijayantha and A. A. Tahir, *J. Am. Chem. Soc.*, 2012, **134**, 1228–1234.
80 A. J. Cowan, C. J. Barnett, S. R. Pendlebury, M. Barroso, K. Sivula, M. Grätzel, J. R. Durrant and D. R. Klug, *J. Am. Chem. Soc.*, 2011, **133**, 10134–10140.
81 B. Iandolo and A. Hellman, *Angew. Chem., Int. Ed. Engl.*, 2014, **53**, 13404–13408.
82 J. H. Kennedy, *J. Electrochem. Soc.*, 1978, **125**, 709.
83 M. P. Dare-Edwards, J. B. Goodenough, A. Hamnett and P. R. Trevellick, *J. Chem. Soc., Faraday Trans. 1*, 1983, **79**, 2027.
84 G. Horowitz, *J. Electroanal. Chem. Interfacial Electrochem.*, 1983, **159**, 421–436.
85 Y. Ling, G. Wang, D. A. Wheeler, J. Z. Zhang and Y. Li, *Nano Lett.*, 2011, **11**, 2119–2125.
86 Y.-S. Hu, A. Kleiman-Shwarsctein, A. J. Forman, D. Hazen, J.-N. Park and E. W. McFarland, *Chem. Mater.*, 2008, **20**, 3803–3805.
87 Y.-S. Hu, A. Kleiman-Shwarsctein, G. D. Stucky and E. W. McFarland, *Chem. Commun.*, 2009, 2652–2654.
88 A. Kleiman-Shwarsctein, Y.-S. Hu, A. J. Forman, G. D. Stucky and E. W. McFarland, *J. Phys. Chem. C*, 2008, **112**, 15900–15907.
89 I. Cesar, K. Sivula, A. Kay, R. Zboril and M. Grätzel, *J. Phys. Chem. C*, 2009, **113**, 772–782.
90 N. T. Hahn and C. B. Mullins, *Chem. Mater.*, 2010, **22**, 6474–6482.
91 V. M. Aroutiounian, V. M. Arakelyan, G. E. Shahnazaryan, H. R. Hovhannisyan, H. Wang and J. A. Turner, *Sol. Energy*, 2007, **81**, 1369–1376.
92 C. X. Kronawitter, S. S. Mao and B. R. Antoun, *Appl. Phys. Lett.*, 2011, **98**, 092108.
93 S. Kumari, A. P. Singh, D. Deva, R. Shrivastav, S. Dass and V. R. Satsangi, *Int. J. Hydrogen Energy*, 2010, **35**, 3985–3990.
94 W. D. Chemelewski, N. T. Hahn and C. B. Mullins, *J. Phys. Chem. C*, 2012, **116**, 5255–5261.
95 P. Zhang, A. Kleiman-Shwarsctein, Y.-S. Hu, J. Lefton, S. Sharma, A. J. Forman and E. McFarland, *Energy Environ. Sci.*, 2011, **4**, 1020.
96 Y. Liu, D.-P. Wang, Y.-X. Yu and W.-D. Zhang, *Int. J. Hydrogen Energy*, 2012, **37**, 9566–9575.
97 J. C. Launay and G. Horowitz, *J. Cryst. Growth*, 1982, **57**, 118–124.
98 R. Shinar and J. H. Kennedy, *Sol. Energy Mater.*, 1982, **6**, 323–335.

99 R. F. G. Gardner, F. Sweett and D. W. Tanner, *J. Phys. Chem. Solids*, 1963, **24**, 1175–1181.
100 S. M. Sze and K. K. Ng, *Physics of Semiconductor Devices*, Wiley, 3rd edn, 2006.
101 Y. Fu, R. Wang, J. Xu, J. Chen, Y. Yan, A. Narlikar and H. Zhang, *Chem. Phys. Lett.*, 2003, **379**, 373–379.
102 P.-S. Li and H. Teng, *J. Chin. Inst. Chem. Eng.*, 2007, **38**, 267–273.
103 T. Lindgren, H. Wang, N. Beermann, L. Vayssieres, A. Hagfeldt and S.-E. Lindquist, *Sol. Energy Mater. Sol. Cells*, 2002, **71**, 231–243.
104 Y. Lin, S. Zhou, S. W. Sheehan and D. Wang, *J. Am. Chem. Soc.*, 2011, **133**, 2398–2401.
105 A. Mao, J. K. Kim, K. Shin, D. H. Wang, P. J. Yoo, G. Y. Han and J. H. Park, *J. Power Sources*, 2012, **210**, 32–37.
106 R. Morrish, M. Rahman, J. M. D. MacElroy and C. A. Wolden, *ChemSusChem*, 2011, **4**, 474–479.
107 H. K. Mulmudi, N. Mathews, X. C. Dou, L. F. Xi, S. S. Pramana, Y. M. Lam and S. G. Mhaisalkar, *Electrochem. Commun.*, 2011, **13**, 951–954.
108 D.-D. Qin, C.-L. Tao, S. In, Z.-Y. Yang, T. E. Mallouk, N. Bao and C. A. Grimes, *Energy Fuels*, 2011, **25**, 5257–5263.
109 S. Rackauskas, A. G. Nasibulin, H. Jiang, Y. Tian, V. I. Kleshch, J. Sainio, E. D. Obraztsova, S. N. Bokova, A. N. Obraztsov and E. I. Kauppinen, *Nanotechnology*, 2009, **20**, 165603.
110 K. Sivula, R. Zboril, F. le Formal, R. Robert, A. Weidenkaff, J. Tucek, J. Frydrych and M. Grätzel, *J. Am. Chem. Soc.*, 2010, **132**, 7436–7444.
111 B. D. Chernomordik, H. B. Russell, U. Cvelbar, J. B. Jasinski, V. Kumar, T. Deutsch and M. K. Sunkara, *Nanotechnology*, 2012, **23**, 194009.
112 V. A. N. de Carvalho, R. A. S. de Luz, B. H. Lima, F. N. Crespilho, E. R. Leite and F. L. Souza, *J. Power Sources*, 2012, **205**, 525–529.
113 S. C. Riha, M. J. D. Vermeer, M. J. Pellin, J. T. Hupp and A. B. F. Martinson, *ACS Appl. Mater. Interfaces*, 2013, **5**, 360–367.
114 S. C. Warren, K. Voïtchovsky, H. Dotan, C. M. Leroy, M. Cornuz, F. Stellacci, C. Hébert, A. Rothschild and M. Grätzel, *Nat. Mater.*, 2013, **12**, 842–849.
115 H. Dotan, O. Kfir, E. Sharlin, O. Blank, M. Gross, I. Dumchin, G. Ankonina and A. Rothschild, *Nat. Mater.*, 2013, **12**, 158–164.
116 S. Linic, P. Christopher and D. B. Ingram, *Nat. Mater.*, 2011, **10**, 911–921.
117 D. B. Ingram and S. Linic, *J. Am. Chem. Soc.*, 2011, **133**, 5202–5205.
118 S. C. Warren and E. Thimsen, *Energy Environ. Sci.*, 2012, **5**, 5133.
119 E. Thimsen, F. le Formal, M. Grätzel and S. C. Warren, *Nano Lett.*, 2011, **11**, 35–43.
120 I. Thomann, B. A. Pinaud, Z. Chen, B. M. Clemens, T. F. Jaramillo and M. L. Brongersma, *Nano Lett.*, 2011, **11**, 3440–3446.
121 H. Gao, C. Liu, H. E. Jeong and P. Yang, *ACS Nano*, 2012, **6**, 234–240.
122 B. Iandolo and M. Zäch, *Aust. J. Chem.*, 2012, **65**, 633.
123 B. Iandolo, T. J. Antosiewicz, A. Hellman and I. Zorić, *Phys. Chem. Chem. Phys.*, 2013, **15**, 4947–4954.
124 C. Du, X. Yang, M. T. Mayer, H. Hoyt, J. Xie, G. McMahon, G. Bischoping and D. Wang, *Angew. Chem., Int. Ed. Engl.*, 2013, **52**, 12692–12695.
125 C. Sanchez, K. D. Sieber and G. A. Somorjai, *J. Electroanal. Chem. Interfacial Electrochem.*, 1988, **252**, 269–290.
126 Z. Chen, H. N. Dinh and E. Miller, *Photoelectrochemical Water Splitting*, Springer, New York, NY, 2013.
127 Ed. H.-J. Lewerenz and L. Peter, *Photoelectrochemical Water Splitting*, Royal Society of Chemistry, Cambridge, 2013.
128 Y. Hou, B. L. Abrams, P. C. K. Vesborg, M. E. Björketun, K. Herbst, L. Bech, A. M. Setti, C. D. Damsgaard, T. Pedersen, O. Hansen, J. Rossmeisl, S. Dahl, J. K. Nørskov and I. Chorkendorff, *Nat. Mater.*, 2011, **10**, 434–438.
129 L. Badia-Bou, E. Mas-Marza, P. Rodenas, E. M. Barea, F. Fabregat-Santiago, S. Gimenez, E. Peris and J. Bisquert, *J. Phys. Chem. C*, 2013, **117**, 3826–3833.
130 F. le Formal, M. Grätzel and K. Sivula, *Adv. Funct. Mater.*, 2010, **20**, 1099–1107.
131 F. le Formal, N. Tétreault, M. Cornuz, T. Moehl, M. Grätzel and K. Sivula, *Chem. Sci.*, 2011, **2**, 737.
132 Y. Matsumoto and E. Sato, *Mater. Chem. Phys.*, 1986, **14**, 397–426.
133 N. Markovic, *Surf. Sci. Rep.*, 2002, **45**, 117–229.
134 C. C. L. McCrory, S. Jung, J. C. Peters and T. F. Jaramillo, *J. Am. Chem. Soc.*, 2013, **135**, 16977–16987.
135 J. Rossmeisl, Z.-W. Qu, H. Zhu, G.-J. Kroes and J. K. Nørskov, *J. Electroanal. Chem.*, 2007, **607**, 83–89.
136 V. Viswanathan, H. A. Hansen, J. Rossmeisl and J. K. Nørskov, *ACS Catal.*, 2012, **2**, 1654–1660.
137 I. C. Man, H.-Y. Su, F. Calle-Vallejo, H. A. Hansen, J. I. Martínez, N. G. Inoglu, J. Kitchin, T. F. Jaramillo, J. K. Nørskov and J. Rossmeisl, *ChemCatChem*, 2011, **3**, 1085.
138 A. Damjanovic, A. Dey and J. O. Bockris, *Electrochim. Acta*, 1966, **11**, 791–814.
139 W. Sheng, H. A. Gasteiger and Y. Shao-Horn, *J. Electrochem. Soc.*, 2010, **157**, B1529.
140 Y. Lee, J. Suntivich, K. J. May, E. E. Perry and Y. Shao-Horn, *J. Phys. Chem. Lett.*, 2012, 399–404.
141 K. Teramura, K. Maeda, T. Saito, T. Takata, N. Saito, Y. Inoue and K. Domen, *J. Phys. Chem. B*, 2005, **109**, 21915–21921.
142 S. D. Tilley, M. Schreier, J. Azevedo, M. Stefik and M. Graetzel, *Adv. Funct. Mater.*, 2014, **24**, 303–311.
143 X. Chen, X. Ren, Z. Liu, L. Zhuang and J. Lu, *Electrochem. Commun.*, 2013, **27**, 148–151.
144 T. Nakagawa, N. S. Bjorge and R. W. Murray, *J. Am. Chem. Soc.*, 2009, **131**, 15578–15579.
145 T. Nakagawa, C. A. Beasley and R. W. Murray, *J. Phys. Chem. C*, 2009, **113**, 12958–12961.
146 S. D. Tilley, M. Cornuz, K. Sivula and M. Grätzel, *Angew. Chem., Int. Ed. Engl.*, 2010, **49**, 6405–6408.

147 M. W. Kanan and D. G. Nocera, *Science*, 2008, **321**, 1072–1075.
148 D. K. Zhong, M. Cornuz, K. Sivula, M. Grätzel and D. R. Gamelin, *Energy Environ. Sci.*, 2011, **4**, 1759.
149 S. C. Riha, B. M. Klahr, E. C. Tyo, S. Seifert, S. Vajda, M. J. Pellin, T. W. Hamann and A. B. F. Martinson, *ACS Nano*, 2013, **7**, 2396–2405.
150 G. Wang, Y. Ling, X. Lu, T. Zhai, F. Qian, Y. Tong and Y. Li, *Nanoscale*, 2013, **5**, 4129–4133.
151 B. Iandolo, B. Wickman, B. Seger, I. Chorkendorff, I. Zorić and A. Hellman, *Phys. Chem. Chem. Phys.*, 2014, **16**, 1271–1275.
152 K. M. H. Young and T. W. Hamann, *Chem. Commun.*, 2014, **50**, 8727–8730.
153 L. Trotochaud, J. K. Ranney, K. N. Williams and S. W. Boettcher, *J. Am. Chem. Soc.*, 2012, **134**, 17253–17261.
154 X. Yang, C. Du, R. Liu, J. Xie and D. Wang, *J. Catal.*, 2013, **304**, 86–91.
155 Y. Hu, D. K. Bora, F. Boudoire, F. Häussler, M. Graetzel, E. C. Constable and A. Braun, *J. Renewable Sustainable Energy*, 2013, **5**, 043109.
156 F. le Formal, K. Sivula and M. Grätzel, *J. Phys. Chem. C*, 2012, **116**, 26707–26720.
157 C. Miao, T. Shi, G. Xu, S. Ji and C. Ye, *ACS Appl. Mater. Interfaces*, 2013, **5**, 1310–1316.
158 D. R. Gamelin, *Nat. Chem.*, 2012, **4**, 965–967.
159 X. Shi, K. Zhang and J. H. Park, *Int. J. Hydrogen Energy*, 2013, **38**, 12725–12732.
160 M. Barroso, C. A. Mesa, S. R. Pendlebury, A. J. Cowan, T. Hisatomi, K. Sivula, M. Grätzel, D. R. Klug and J. R. Durrant, *Proc. Natl. Acad. Sci. U. S. A.*, 2012, **109**, 15640–15645.
161 G. M. Carroll, D. K. Zhong and D. R. Gamelin, *Energy Environ. Sci.*, 2015, **8**, 577–584.
162 T. Hisatomi, F. le Formal, M. Cornuz, J. Brillet, N. Tétreault, K. Sivula and M. Grätzel, *Energy Environ. Sci.*, 2011, **4**, 2512.
163 L. Xi, P. S. Bassi, S. Y. Chiam, W. F. Mak, P. D. Tran, J. Barber, J. S. Chye Loo and L. H. Wong, *Nanoscale*, 2012, **4**, 4430–4433.
164 L. Xi, S. Y. Chiam, W. F. Mak, P. D. Tran, J. Barber, S. C. J. Loo and L. H. Wong, *Chem. Sci.*, 2013, **4**, 164.
165 M. Zhang, W. Luo, N. Zhang, Z. Li, T. Yu and Z. Zou, *Electrochem. Commun.*, 2012, **23**, 41–43.
166 D. Cao, W. Luo, M. Li, J. Feng, Z. Li and Z. Zou, *CrystEngComm*, 2013, **15**, 2386.
167 Y. Cong, M. Chen, T. Xu, Y. Zhang and Q. Wang, *Appl. Catal., B*, 2014, **147**, 733–740.
168 J. Y. Kim, H. Jun, S. J. Hong, H. G. Kim and J. S. Lee, *Int. J. Hydrogen Energy*, 2011, **36**, 9462–9468.
169 R. Franking, L. Li, M. A. Lukowski, F. Meng, Y. Tan, R. J. Hamers and S. Jin, *Energy Environ. Sci.*, 2013, **6**, 500.
170 C.-Y. Lee, L. Wang, Y. Kado, R. Kirchgeorg and P. Schmuki, *Electrochem. Commun.*, 2013, **34**, 308–311.
171 T. Hisatomi, H. Dotan, M. Stefik, K. Sivula, A. Rothschild, M. Grätzel and N. Mathews, *Adv. Mater.*, 2012, **24**, 2699–2702.
172 D. Wang, X.-T. Zhang, P.-P. Sun, S. Lu, L.-L. Wang, Y.-A. Wei and Y.-C. Liu, *Int. J. Hydrogen Energy*, 2014, **39**, 16212–16219.
173 F. Meng, J. Li, S. K. Cushing, J. Bright, M. Zhi, J. D. Rowley, Z. Hong, A. Manivannan, A. D. Bristow and N. Wu, *ACS Catal.*, 2013, **3**, 746–751.
174 T.-Y. Yang, H.-Y. Kang, K. Jin, S. Park, J.-H. Lee, U. Sim, H.-Y. Jeong, Y.-C. Joo and K. T. Nam, *J. Mater. Chem. A*, 2014, **2**, 2297.
175 F. le Formal, M. Grätzel and K. Sivula, *Adv. Funct. Mater.*, 2010, **20**, 1099–1107.
176 J. Deng, X. Lv, J. Gao, A. Pu, M. Li, X. Sun and J. Zhong, *Energy Environ. Sci.*, 2013, **6**, 1965.
177 N. T. Hahn, H. Ye, D. W. Flaherty, A. J. Bard and C. B. Mullins, *ACS Nano*, 2010, **4**, 1977–1986.
178 C. X. Kronawitter, S. S. Mao and B. R. Antoun, *Appl. Phys. Lett.*, 2011, **98**, 092108.
179 G. Rahman and O.-S. Joo, *Int. J. Hydrogen Energy*, 2012, **37**, 13989–13997.
180 O. Zandi, B. M. Klahr and T. W. Hamann, *Energy Environ. Sci.*, 2013, **6**, 634.
181 O. Zandi, J. A. Beardslee and T. Hamann, *J. Phys. Chem. C*, 2014, **118**, 16494–16503.
182 O. Zandi and T. W. Hamann, *J. Phys. Chem. Lett.*, 2014, **5**, 1522–1526.
183 P. Zhao, C. X. Kronawitter, X. Yang, J. Fu and B. E. Koel, *Phys. Chem. Chem. Phys.*, 2014, **16**, 1327–1332.
184 L. Wang, C.-Y. Lee, A. Mazare, K. Lee, J. Müller, E. Spiecker and P. Schmuki, *Chemistry*, 2014, **20**, 77–82.
185 T. Wang, M.-C. Huang, Y.-K. Hsieh, W.-S. Chang, J.-C. Lin, C.-H. Lee and C.-F. Wang, *ACS Appl. Mater. Interfaces*, 2013, **5**, 7937–7949.
186 Y. Lin, Y. Xu, M. T. Mayer, Z. I. Simpson, G. McMahon, S. Zhou and D. Wang, *J. Am. Chem. Soc.*, 2012, **134**, 5508–5511.
187 M. K. Nowotny, T. Bak and J. Nowotny, *J. Phys. Chem. B*, 2006, **110**, 16270–16282.
188 M. K. Nowotny, L. R. Sheppard, T. Bak and J. Nowotny, *J. Phys. Chem. C*, 2008, **112**, 5275–5300.
189 B. Iandolo, H. Zhang, B. Wickman, I. Zorić, G. Conibeer and A. Hellman, *RSC Adv.*, 2015, DOI: 10.1039/C5RA10215D.

